Materials Sciences Corporation

DEVELOPMENT OF AN ANALYTIC PROCEDURE TO CALCULATE DAMAGE ACCUMULATION IN COMPOSITES DURING LOW VELOCITY IMPACT

Technical Final Report
MSC TFR 1315/0208
February, 1983

Prepared by:
E. A. Humphreys and J. Goering

Prepared for:
National Aeronautics and Space Administration
Langley Research Center
Hampton, Virginia

Gwynedd Plaza II, Bethlehem Pike, Spring House, PA • 215-542-8400

DEVELOPMENT OF AN ANALYTIC PROCEDURE TO CALCULATE DAMAGE ACCUMULATION IN COMPOSITES DURING LOW VELOCITY IMPACT

E. A. HUMPHREYS AND J. GOERING

Materials Sciences Corporation

SUMMARY

This report describes the second phase of an analytical effort to model the effects of low velocity transverse normal impact on laminated composite plates. The methodology utilized consisted of a transient dynamics finite element analysis with capabilities for composite material characterization and stress predictions. A shear flexible plate bending element with material bending/extensional coupling capabilities was developed for this effort. The contact effects between the impacting mass and composite plate were modelled utilizing a nonlinear contact spring similar to Hertzian contact. Provisions were included for incorporating the effects of both ply damage and delaminations through modifications to the element stiffness matrices.

An impact analysis was performed to simulate the impact of a steel sphere on an eight ply, quasi-isotropic graphite/epoxy plate. The response of the plate and impactor were modelled through 100 μsec of the impact event. Damage predicted included both matrix cracking and fiber breakage within the composite plate. Damage was shown to be a function of high flexural modes present early in the impact event.

FOREWORD

This report summarizes the work performed under contract NAS1-15888 for the NASA Langley Research Center during the period August 3, 1979 to April 15, 1983. Mr. Walter Illg was the NASA Technical Representative and the authors wish to express their appreciation to him for the many technical inputs provided by him and by Dr. Wolf Elber.

The Program Manager for MSC was Dr. B. Walter Rosen and the Principal Investigator was Mr. E. A. Humphreys. Mr. J. Goering performed all of the software development and analyses.

TABLE OF CONTENTS

INTRODUCTION

With the ever increasing use of laminated composites in structural applications, an interesting phenomenon has become apparent. This phenomenon concerns the real possibility of invisible damage within a composite structure caused by low velocity, low mass impacts. This type of loading environment is most easily envisioned as the impact of a dropped workman's tool on a structure or, perhaps, runway debris ejected onto a structure.

The primary concern related to this type of loading environment is the introduction of performance degrading damage within the composite structure. This damage may not be visually apparent during subsequent inspections of the structure and, hence, the performance degradation will also not be immediately apparent.

The subject of impact related phenomena has been studied by many investigators utilizing many different approaches. Much of this work has been related to ballistic type impact and, hence, is not applicable here. In ballistic impact, the velocities involved are high enough to promote large stress wave propagation effects.

Prior work in the analysis of the low speed impact problem has established that it is reasonable to neglect the stress wave propagation problem and to focus on the transient structural dynamic approach. Different approaches have appeared in the literature to combine contact effects with dynamic effects. The Hertz contact problem has been extended to the problem of dynamic contact and also to the problem of contact of anisotropic bodies (see ref. 1). These approaches treat impact with a semi-infinite target. In the present case, one is concerned with a target in which the dynamic response of the target is important in the sense of transient structural motion rather than material displacement. This problem appears to have been addressed first by Timoshenko (ref. 2), as described by Goldsmith (ref. 3). Timoshenko studied the problem of the impact of a beam where the contact between the bodies was governed by Hertz's law for contact deformations. Karas (ref. 4) extended the Timoshenko approach to the study of plate impact (see

ref. 5). Moon (refs. 6 and 7) has utilized the Hertz impact theory in combination with a Mindlin plate theory (ref. 8) to model a similar approach for impact of plate structures. This particular approach yields a nonlinear mathematical problem and extended numerical analysis is required to obtain solutions. The procedure is sufficiently complex to motivate consideration of alternate approaches.

Two such approaches are based on simplifications of the contact force analysis. In one case, it is considered that the impact takes place during a time period which is very short compared to the period of the first natural frequency. In this case, it appears reasonable to regard the impact as having imparted an impulse locally to the plate and to then study the dynamic response of the composite plate target to that impulsive loading. This approach (see ref. 9) is appropriate as the structural stiffness increases and the impacting mass decreases.

Another line of approach initiated by Clebsch (ref. 10) as described by Goldsmith (ref. 3) assumes that upon impact, the projectile moves with the plate and that the velocity of the projectile becomes an initial velocity condition. Thus, the analysis is the structural dynamic response of the plate with the attached mass. McQuillen et al. (ref. 11) applied this approach to a beam. They minimized some of the numerical problems by considering the contact zone between projectile and target to have finite width. This approach tended to minimize the contribution of the higher frequency modes and, thus, numerical procedures were more successful. However, even with these assumptions, the work of reference 11 shows that modes of vibration other than the fundamental mode can be excited by impact, particularly if the striker mass is small. This approach, which is expanded somewhat in references 12 and 13, is being utilized in the current effort.

In the present study, the primary emphasis has focused on the prediction of damage initiation and propagation during the impact event and subsequent dynamic plate response. The difficulty posed here is that any induced damage will alter the plate stiffness locally and, hence, affect the subsequent dynamic response. Thus, the closed form analytical approach taken in references 11-13 is not applicable.

In the first phase of the current effort (ref. 14), a classical thin shell finite element transient dynamics analysis (ref. 15) was coupled with lamination theory to predict the flexural response of composite plates subjected to transverse impact. The impact was assumed to be perfectly plastic with the impactor mass lumped at specified nodes within the finite element model. Both layer and interlaminar damage were predicted using a stress based failure criterion. The effects of impact induced damage were included by modifying the local, elemental stiffness matrices to reflect the loss of ply stiffness. No stiffness reductions were possible for interlaminar damage because the model did not include the effects of shear deformation.

In this second phase, the transient structural dynamics model with stiffness modifications to account for damage has been retained. The model has been extended to incorporate nonlinear contact effects between the impactor mass and the plate structure. This effort reflects the desire to model the energy transfer mechanisms and energy loss which occur at the point of impact and utilized the work of Sun and Yang (refs. 16 and 17).

In addition to the contact effects, the structural dynamics model has been extended to include the effects of shear deformation. This required a new shear flexible plate bending finite element derived from the work of Hinton et. al. (ref. 18) and transverse shear constitutive relations developed by Cohen (ref. 19).

The computerized procedure has been utilized to predict the response of a laminated plate subjected to a low velocity impact event. Structural response including damage initiation and growth has been predicted and is documented within this report.

ANALYTICAL METHODOLOGY

The transient dynamic analysis of laminated composite plates subjected to low velocity impact can be broken into three interrelated procedures: stiffness formulation, displacement solution and laminate stress/failure analysis. The stiffness of the model depends on the failure status of the laminate; the displacement solution depends upon the stiffness of the model; and, the state of stress in the model depends upon the displacement field. The stress state defines the failure status of the laminate which redefines the stiffness of the model, and the process continues.

The analysis begins with the formulation of the stiffness for an undamaged laminate, using conventional finite element techniques. The finite element, which has been developed for use in CLIP II, is an eight noded isoparametric quadrilateral with cubic displacement functions. This element possesses both plate bending and membrane displacements, and includes shear deformation effects and the ability to handle materials with bending-extensional coupling. These features make it an ideal element for the study of thin and thick laminated shells which need not be balanced or symmetric. The theoretical details of the formulation of this element are included in Appendix A.

Being a dynamic analysis, the mass and damping matrices for the systems are also required. A diagonal (lumped) mass matrix is used, which includes rotary inertia terms. As the analysis proceeds, the stiffness of any individual element may change to reflect the effects of ply damage and delaminations; the mass matrix, however, remains unchanged throughout. It is assumed that the damping matrix is a linear combination of the mass and stiffness matrices (Rayleigh damping) and will therefore change in accordance with changes in stiffness.

To completely describe the mass and stiffness of the dynamic system, the mass and contact stiffness of the impactor must also be known. The impactor is treated as a lumped mass that is tied

to the plate at a single node by a nonlinear contact spring. The nonlinear contact spring contains hysterisis, and its stiffness vanishes if the plate and impactor have separated. Details of the contact spring are given in Appendix B.

With the mass, damping and stiffness of the system known, the equations of motion may be integrated to yield nodal displacements, velocities and accelerations as functions of time. CLIP II performs this integration numerically, using the fourth order Runge-Kutta-Gill method. The R-K-G method is a very accurate algorithm, but has the disadvantage of being sensitive to all dynamic modes of the system. This may require that a relatively small time step size be used to insure stability.

The procedure is started by specifying the initial conditions, both displacements and velocities, of the system. CLIP II has provisions for specifying nonzero initial conditions for the plate and the impactor. Note that gravity is not included in the model, therefore an impactor that is given an initial displacement with no initial velocity will not "fall" on the plate.

A restart capability has also been included in the code. When a restart analysis is performed, the last solution is read from storage and used as the initial conditions for subsequent solutions. The time increment used in the restart analysis may be different than that used in the original analysis. This capability allows the analysis to be stopped and restarted with a larger time increment after higher frequency modes have damped out of the problem.

An option to correct the dynamic solution after a specified number of time steps has been included. This is done using Hamming's fourth order corrector algorithm. This algorithm is an implicit scheme which uses information from the last three time steps to correct the solution at the present time. Being an implicit scheme, it must be used iteratively, which may become very time consuming. It is typically more cost effective to improve the accuracy of the results by reducing the size of the time increment in the R-K-G procedure, rather than evoking this correcting algorithm. Hamming's method also requires that the time increment be

constant for the three time steps prior to the current time step, which may prohibit its use on some solutions. The R-K-G method, Hamming's algorithm, and their implementation in CLIP II are discussed in further detail in Appendix C.

The displacement solution at any time step may be used to perform a laminate stress analysis on an element by element basis. The strains at the centroid of an element are found by averaging the strains calculated at the Gauss points for the element in question. These are computationally efficient points to use, since the strain-displacement relationships have already been evaluated there during the stiffness formulation. These strains and curvatures are found in the global coordinate system, and must be transformed into material coordinates on a ply by ply basis.

Stresses are calculated at the bottom, mid-plane and top surfaces of each ply. These stresses are then used to predict ply damage or delaminations between plies. The failure criteria used in CLIP II are listed in Appendix D. These criteria predict both the presence of failure and the mode of failure.

The mode of failure determines how the element stiffness matrix will be modified to reflect the effects of the predicted damage. Ply failures and delaminations are handled in radically different ways. Ply failures are incorporated by modifying the material properties of individual lamina, whereas delaminations are included by modifying the fundamental strain-displacement relationships for the element.

The way in which the lamina properties are changed depends upon the type of ply damage. If the ply damage includes fiber failure, then the entire ply is removed from the laminate. If matrix failure is the only failure mode, it is assumed that the fiber can still carry load; thus, only the transverse properties of the ply are removed. These laminate modifications apply only to the specific element under consideration. Damage in one element will, therefore, not affect the stiffness of other elements.

Delaminations pose a more difficult problem. CLIP II incorporates delaminations by modifying the strain-displacement relationship to reflect the effects of singular forces in the plane of the delamination. The magnitude of this force can be expressed in terms of the displacement functions and the constitutive relations for the laminate, which allows it to be incorporated in the finite element scheme. The details of this approximate procedure are included in Appendix E. Unfortunately, the formulation used for incorporating delaminations in the analysis places some severe restrictions on the geometry of the element. Only rectangular elements may be used, and they must be oriented as shown in figure 1.

Upon completion of the laminate analysis, the stiffness of the model is modified to reflect any damage that may have been predicted. The dynamic analysis then proceeds at this reduced stiffness until further damage is predicted by the laminate analysis and additional stiffness reduction is performed. This procedure continues until the desired number of time steps has been reached, or an element suffers complete failure.

IMPACT ANALYSES

The impact analysis code described earlier has been utilized to predict the response of 10.16 cm x 15.24 cm rectangular clamped-clamped graphite epoxy plate. The laminate is comprised of T-300/5208 material arranged in a $[45/0/-45/90]_s$ layup. The material elastic and strength properties utilized are listed in table 1. The laminate total mass was 25.3 g with a total thickness of 0.1057 cm.

The impact event modelled corresponds to a 1.59 cm steel sphere (16.45 g) impacting the plate centrally with a velocity of 9.4 m/s. The various coefficients required to define the response of the contact between the plate and impacting sphere were determined utilizing data from references 16 and 17 and are listed in table 2.

CHARACTERIZATION OF IMPACT RESPONSE

An initial analysis was performed without stress calculation in order to determine both the characteristics of the impact event and verify the workings of the CLIP II code. This analysis also provided information relating to the time step required for numerical stability of the R-K-G solution procedure.

The finite element model used in the initial analysis is shown in figure 2. This model is rather crude but still provides a reasonable displacement response and yielded the required information. Since no stress analysis was included, the analysis yielded the elastic response of an undamaged plate.

The dynamic response was initiated with an integration time step of 0.1 μsec. After approximately 10 μsec, the time step was gradually increased until a maximum time step of 0.25 μsec was found. Above 0.25 μsec, the solution procedure became numerically unstable and divergent. This very short time step requirement stems from the sensitivity of the solution procedure to all possibly dynamic modes present in the model. In the solution where the

integration time step was larger than 0.25 μsec, the rotational degrees of freedom appeared to become unstable first indicating either high bending modes and/or transverse shear effects were causing the difficulty. When the time step was specificed to be 0.25 μsec, no difficulties were encountered and the plate response was monitored out to 750 μsec. This period of time was long enough to include the maximum lateral deflection of the plate and hence characterize the plate response to the impact event.

The lateral deflection of the node at which the impact occurs, and the displacement of the impactor have been plotted as functions of time in figure 3. Notice that the impactor follows a smooth, almost sinewave like curve, while the center of the plate travels an irregular path. This implies that higher dynamic flexural modes are combining with the fundamental flexural mode to define the response of the plate.

Although the mass of the entire plate is of the same order of magnitude as the impactor, the effective mass of the portion of the plate which undergoes substantial motion is far less than that of the impactor. Thus, by conservation of momentum, it is possible for the plate to achieve a velocity which will allow it to separate from the impactor.

Separation of the plate and impactor occurs three times during the time interval analyzed. In figure 4, separation of the plate and impactor is seen to occur from approximately 100 to 170 μsecs, again from approximately 280 to 440 μsecs and finally from 540 to 560 μsecs. During each of these intervals, the plate moves under the action of inertial forces alone since the contact force between the plate and impactor has vanished.

Referring back to figure 3, the plate/impactor separation during the period 280 to 440 μsecs is readily apparent. During the other two separation intervals, the total separation distance is smaller than the permanent deformation which has occurred in the plate due to the contact of the impactor. Hence, the loss of contact cannot be seen directly.

When contact is lost, the impactor is in "free fall" (constant velocity), until contact is regained, once again causing the impactor to lose velocity. The impactor continues to slow down until approximately 650 μsec into the event. At this time, the plate begins to act like a compressed spring which releases its energy by pushing the impactor back in the direction from which it came. The velocity of the impactor passes through zero and changes sign. It will continue to pick up speed until it is thrown free from the plate, ending the event.

The displacement response very early in the impact event is depicted in figure 5. Displacements through the center of the plate along the longer dimension are shown at 25 μsec to 100 μsec. Throughout this period of time, the plate response is easily seen to be dominated by flexural modes other than the fundamental mode of the clamped-clamped plate. At 100 μsec, the maximum plate deflection is approximately 75% of the plate thickness. This would indicate that the flexural response is still the dominant load carrying mechanism at 100 μsec. Referring to figure 3, the maximum displacement is seen to approach the plate thickness at approximately 125 μsec. As the maximum displacement becomes larger than the plate thickness, the stiffness of the plate will increase as large deflection membrane action becomes significant.

Since the analysis performed is strictly linear, these effects are not included. Hence, beyond approximately 125 μsec the accuracy of the predicted response must be considered suspect. The trends which have been shown are believed to be representative of the impact event. The multimode flexural response is apparent long before the plate displacements reach the plate thickness indicating no significant membrane response involvement. The first plate/impactor separation occurs when the plate displacement is approximately equal to the plate thickness. Thus, even though membrane stretching is present, it is not the dominant response.

STRESS AND FAILURE PREDICTIONS

Having characterized the displacement response of the clamped plate, a second analysis was performed in order to predict stresses and damage within the plate due to the impact event. A new finite element mesh was developed since the size of the individual element in the mesh of figure 2 precluded realistic stress prediction. The finite element model utilized for stress and failure predictions is depicted in figure 6. The shaded elements in figures 6 were monitored for stress and damage.

The refined model contains 521 unconstrained nodal points with three bending degrees of freedom per node. In addition, in-plane membrane degrees of freedom were retained in order to model any bending/extensional coupling introduced due to unsymmetric damage. Thus, the refined model contained 2605 active degrees of freedom.

The inclusion of significantly more elements and degrees of freedom in the mesh introduced significantly higher flexural frequencies into the possible nodes of the model. As was stated previously, the solution algorithm utilized is sensitive to all possible dynamic nodes in the model. Thus, the maximum integration time step was reduced in comparison to the model utilized for the displacement only model. In the analysis performed with the refined model, a time step no larger than 0.1 μsec was required for numerical stability.

Utilizing the finite element mesh of figure 6 and identical laminate and impact conditions as used previously, displacement, stress and damage were predicted for 100 μsec into the impact event. Using time step of 0.1 μsec, the analysis was performed for 1000 time increments. In the analysis, stresses were computed every 5 μsec or every 50 time steps.

The lateral displacements of the impactor and node on the plate, which the contact spring is attached to, are plotted in figure 7. The impact mass is seen to be displacing along a

smooth path while the path of the plate is slightly irregular. This is similar to the type of response predicted with the coarse model. Comparing figure 7 and the first 100 μsec plotted in figure 3, the two finite element meshes are seen to yield similar displacement-time responses.

The displacement response of the plate through 100 μsec is depicted in figures 8 and 9. The displacements are plotted for lines through the plate center with figure 8 corresponding to the larger chord of the plate and figure 9 the shorter chord. Comparison of figures 5 and 8 demonstrates that the coarse and refined finite element meshes yield the same maximum displacements for the plate. The curvatures produced in the refined mesh are significantly larger, however.

The presence of high flexural nodes is easily discernable in figures 8 and 9. The plate response is seen to begin with a highly localized deformation at the point of impact. As the deformation continues, it takes on the shape of a flexural wave spreading from the point of contact to the plate boundaries. As the wave passes through a point on the plate, the local curvatures reverse in sign. This is graphically demonstrated in figure 10 where fiber direction stresses in the bottom 45° ply are depicted as a function of time. The stresses are plotted for element 79. The position in the nodel of element 79 can be found in figure 11 where the finite element mesh is reproduced with element numbers included.

The stresses in figure 10 are seen to be compressive from the start of the impact event through approximately 33 μsec. The negative stresses during this period are due to the reversed curvatures which can be seen in figures 8 and 9. Beyond 33 μsec, the depicted stresses become positive and remain positive for the remainder of the 100 μsec analysis. At the point in time where the fiber direction stresses in the back ply of element 79 become zero, the same ply in adjacent elements have either positive or negative stresses depending upon their position relative to the

spreading flexural wave. At 33 μsec, the advancing flexural wave is located such that in element 79 the back 45° ply is unstressed in the direction of the fiber. Beyond 33 μsec, the stresses in the back ply of element 79 become positive and oscillate somewhat due to the presence of high flexural modes and possibly induced damage.

Damage which was predicted in the 100 μsec analysis is depicted in figure 12. Only those elements which were monitored for stress and damage are included in figure 12. Thus, the elements represented in figure 12 correspond to the shaded elements depicted in figure 6. Damage is first predicted at 35 μsec. At this time, the four elements surrounding the point of impact have experienced some damage. Elements 90 and 103 have experienced fiber failure in ply 1 (back face 45° ply) and matrix failure in ply 2 (0° ply). Elements 91 and 102 have experienced matrix failure in ply 1 at 35 μsec.

The occurrence of fiber failure in the back 45° ply of elements 90 and 103 is interesting when compared with the fiber direction stresses of the back 45° ply of element 79 depicted in figure 10. Figure 10 indicates that at 35 μsec the ply 1 fiber direction stress in element 79 is less than 10 MPa while the same ply in elements 90 and 103 has failed in the fiber direction. The large difference in the stress state between these locations is due to the location of the spreading flexural wave. Since at 35 μsec the transition from compression to tension has only just passed element 79, low stresses are to be expected. Elements 90 and 103 are adjacent to the impact site where curvatures are maximum and, hence, the stresses there can be expected to be large.

Returning to figure 12 and the progression of impact induced damage, it is seen that at 40 μsec, elements 91 and 103 have experienced matrix failure in ply 3. Ply 3 is oriented at -45° and is below the midsurface. Since ply 3 is oriented at 90° with respect to ply 1, the induced matrix failure suggests a similar loading state which promotes fiber failure in ply 1 at 35 μsec.

The combination of curvatures which produced large fiber direction stresses in ply 1 will produce stresses perpendicular to the fiber in ply 3 and, hence, matrix failure occurs in ply 3.

The combined effects of compressive strengths being larger than tensile strengths and shifting of the neutral surface upward due to damage below the midplane, delays the onset of damage above the midsurface until 45 μsec. At this time, elements 90 and 103 experience fiber failure in ply 8 (top 45° ply). The laminate remains in this damage state until 70 μsec have elapsed in the impact event.

At 70 μsec into the impact event, matrix damage in ply 2 spreads to elements 91 and 102. Ply 2 experiences additional matrix mode damage in elements 78 and 115 at 80 μsec. At 90 μsec, matrix mode damage occurs in ply 1 of elements 79 and 114. Finally, at 100 μsec, ply 2 experiences additional matrix mode damage in elements 79 and 114. The progression of damage from the four elements surrounding the impact site (90, 91, 102, 103) to elements further away (78, 79, 114, 115) reflects the spreading of the flexural wave and the effects of included damage on subsequent plate response. The progression of damage in the 100 μsec analysis is summarized in tables 3 and 4. Although interlaminar shear stresses were found to be as high as approximately 28 MPa, no delaminations were predicted during the 100 μsec analysis.

DISCUSSION

The impact analyses performed have generated information leading to a better understanding of the impact response of thin composite plates. The most interesting feature brought out in these analyses is the introduction of damage very early in the impact event.

The displacement fields which were depicted in figures 8 and 9 demonstrated that at times less than 100 μsec, the plate responded with very high local curvatures at the point of impact. These large curvatures produced considerable local damage. As the impact event progressed, the displaced shapes of the plate began to approach what appeared to be the fundamental flexural mode of the clamped-clamped plate. The damage had appeared before the fundamental mode could be attained, however. Thus, when the plate response degenerates into this mode, the properties of the plate have changed from its virgin state. This indicates that the first mode response of the plate must be different in the impact event than it would be under static or quasi-static loading since static static loads cannot produce the very high local curvatures and resultant damage.

The prediction of damage in the current analyses is considerably different than that experienced in the first phase of this effort (ref. 14). In both models, the planar area of damage was approximately 1.0 cm x 1.5 cm. In the earlier effort, the analyses predicted such extensive damage at the point of impact that the elemental stiffness matrices became singular. Additionally, the damage occurred earlier such that the maximum time in the solution was 75 μsec. The current analysis produced much less damage through the plate thickness.

The damage predicted in the current effort more closely simulates the damage produced experimentally in tests performed at NASA Langley than did the earlier effort. The impact parameters and laminate configuration used in the analyses were pre-

scribed to analyze experimental work from which qualitative damage descriptions were available. The experimental work produced matrix damage and delaminations but not significant fiber damage. Thus, the earlier model severely over predicted the extent of damage. The current analysis predicted much less extensive damage and, hence, more closely predicted the experimental work.

The primary reason for the reduction in the extent of predicted damage relates to the way in which the impact load is introduced into the plate. In the earlier effort, the impact mass was lumped at nodes of the plate and given an initial velocity. Thus, a step loading was applied. In the current model, a nonlinear contact spring is utilized. This allows for a more realistic gradual introduction of load. The contact spring stiffness is initially zero but increases with increasing displacement of the impactor relative to the plate.

Another factor which must be considered is the relative sizes of the individual elements surrounding the impact site. Although the two models contained similar numbers of flexural degrees of freedom (1953 earlier effort, 1563 current effort), the current element requires midsize nodes. Therefore, fewer elements can be included for the same number of degrees of freedom. Thus, in the earlier effort, the elements at the impact site were approximately 0.16 cm x 0.16 cm while in the current effort the impact site elements were approximately 0.42 cm x 0.42 cm. Therefore, some of the local stress response may have been lost in the current effort. It is believed that element size caused the lack of interlaminar damage in the current effort.

The obvious solution to this problem would be to increase the number of finite elements in the model and decrease the size of the elements local to the impact site. The difficulty is the magnitude of the finite element model that this would induce. In the current model, there were 2605 active degrees of freedom (including in-plane displacements) yielding 5210 simultaneous

differential equations (see Appendix C). This model approached the maximum size which was pratical to work with.

The removal of in-plane degrees of freedom would significantly reduce the size of the problem while eliminating any bending/extensional coupling effects. This could be accomplished in a clamped plate by reformulating the laminate bending properties to enforce bending about the neutral rather than midsurface. Such a modification would be more difficult to define for a simply supported plate.

The size of the current solution was one reason for terminating the analysis at 100 μsec. As was stated, this corresponded to 1000 time increments. The current analysis is very costly to execute which must be considered typical of transient dynamics analyses. In addition to the time and expense of operating the code, the displacements at 100 μsec were approaching 75% of the plate thickness. The validity of the solution becomes suspect as the displacements reach the plate thickness and membrane stretching effects come into play. For the eight ply laminate utilized in the analysis, it can be expected that membrane effects will become significant if not dominant at times later than 100 μsec. Since the analysis cannot handle large deflection effects, it was deemed prudent to stop the analysis at 100 μsec.

RECOMMENDATIONS

The impact analysis methodology which has been incorporated into the CLIP II computer code has identified some significant phenomena regarding low velocity impact of thin composite laminates. Specifically, significant damage producing curvatures have been identified at times very early in the impact event. This type of deformation, which is characteristic of very high dynamic flexural mode exitation, has been shown to promote damage within the first 100 μsec of a typical impact event. The transient dynamics finite element analysis has proven to be costly, however, and therefore future efforts should be directed towards defining realistic simplifications to the analysis in order to obtain a practical design/analysis tool.

The results obtained utilizing the CLIP II code can be seen to indicate two distinct modes of plate response and, hence, damage producing mechanisms. In the very early stages of an impact event, very high frequency flexural effects dominate the response. At considerably later times, the plate response degenerates into what appears to be a fundamental flexural mode response, possibly coupled with large deflection effects. The significance of the large deflection membrane response will be determined both by the characteristics of the plate (i.e. thickness) and the impactor energy and velocity. Simplifications to the impact analysis will necessarily be directed towards these two regimes independently.

The early response of a thin plate subjected impact loading is characterized by high local curvatures. This type of response should be present in impact of thicker plates although perhaps not as pronounced. Simplifications of early time response analysis should take advantage of the localized nature of the high curvatures. Early in the impact event, significant portions of the plate are unaffected. As the event progresses, the portion of the plate which is unaffected decreases until finally the entire plate is deforming. It should be possible to define characteristic dimensions of the plate as functions of time corresponding to the

deformed regions of the plate. This information could then be used to reduce the size of the required finite element model. Alternately, this data could be utilized to develop one-dimensional models where a first mode solution would be used to model the deformations of the affected regions of the plate. Either of these approaches should greatly reduce the time and cost of performing the analyses for early time response.

The later time response might be simulated using a first mode flexural analysis with large deflection capabilities. The models would need to include the effects of any damage which occurred during the early times of the impact event. This approach would require that late time plate response does, in fact, degenerate into the fundamental mode of the plate structure.

Simplifications of either short or long term impact response will require considerable study of impact phenomena. Realms of applicability of possible simplifications must be defined in order that the analyses be realistic. The information to be gathered could be obtained experimentally or analytically. Experimental efforts would need to monitor the plate response in such a way as to yield both displacement vs. time and displacement vs. position. Analytical efforts would also have to characterize the time-position characteristics of the displacement response.

The types of analysis simplifications described would allow for the development of cost effective design/analysis tools which could be utilized to investigate impact events. The current methodology must be considered too costly to be utilized routinely. Simplified analytical methodologies with known limitations would be a valuable contribution in the continuing study of low velocity impact.

REFERENCES

1. Willis, J. R., "Hertzian Contact of Anisotropic Bodies," Journal of Mechanics of Physical Solids, Vol. 14, 1966, pp. 163-176.
2. Timoshenko, S. P., "Zur Frage nach der Wirkung eines Stosses auf einer Balken," Z. Math. Phys., Vol. 62, 1913, No. 2, p. 198.
3. Goldsmith, W., Impact. E. Arnold Ltd. (Publishers) 1960, Chapter IV.
4. Karas, K., "Platten Unter Seitlichem Stoss," Ingenieur-Archiv, Vol. 10, 1939, p. 237.
5. Sun, C. T., and Chattopadhyay, S., "Dynamic Response of Anisotropic Plates Under Initial Stress due to Impact of a Mass," Trans. A.S.M.E., J. Appl. Mech., Vol. 42, 1975, p. 693.
6. Moon, F. C., "Wave Surfaces Due to Impact on Anisotropic Plates," Journal of Composite Materials, Vol. 6, 1972, p. 62.
7. Moon, F. C., "Theoretical Analysis of Impact in Composite Plates," NASA CR-12110, Princeton University, 1973.
8. Mindlin, R. D., "High Frequency Vibrations of Crystal Plates," Quarterly of Applied Mathematics, Vol. 19, 1961, p. 51.
9. Chou, P. C., Flis, W. J. and Miller, H., "Low Speed Impact of Plates of Composite Materials," NADC 78259-60, 1978.
10. Clebsch, A., Theorie de l'elasticite des corp solides, trans. B. de St.-Venant and M. Flamant, Dunod, Paris, 1883.
11. McQuillen, E. J., Llorens, R. E., and Gause, L. W., "Low Velocity Transverse Normal Impact of Graphite-Epoxy Composite Laminates," Report No. NADC-75119-30, Naval Air Development Center, Warminster, PA, June 1975.
12. Chou, P. C., Flis, W. J. and Miller, H., "Certification of Composite Aircraft Structures under Impact Fatigue, and Environmental Conditions. Part I. Low Speed Impact of Plates of Composite Materials," NADC-78259-60, January 1978.
13. Llorens, R. E., McQuillen, E. J., "Off Center, Low Velocity, Transverse Normal Impact of a Viscoelastic Beam," NADC-78237-60, September 1978.

14. Humphreys, E. A., "Development of an Engineering Analysis of Progressive Damage in Composites During Low Velocity Impact," NASA CR-165778, July 1981.
15. Bathe, K. J., Wilson, E. L., Peterson, F. E., "SAP IV, A Structural Analysis Program for Static and Dynamic Response of Linear Systems," EERA 73-11, June 1973.
16. Sun, C. T. and Yang, S. H., "Contact Law and Impact Responses of Laminated Composites," NASA CR-159884, February 1980, Purdue University.
17. Yang, S. H. and Sun, C. T., "Indentation Law for Composite Laminates," NASA CR-165460, July 1981, Purdue University.
18. Hinton, E., Razzaque, A., Zienkiewicz, O. C., and Davies, J. D., "A Simple Finite Element Solution for Plates of Homogeneous, Sandwich and Cellular Construction," Proc. Instn. Civ. Engrs., Part 2, March 1975, 59, pp. 43-65.
19. Cohen, G. A., "Transverse Shear Stiffness of Laminated Anisotropic Shells," Computer Methods in Applied Mechanics and Engineering," Vol. 13, 1978.
20. Irons, B. and Ahmad, S., "Techniques of Finite Elements," 1980, John Wiley & Sons, New York, NY.
21. Zienkiewicz, O. C., "The Finite Element Method," 1977, McGraw-Hill, Maidenhead, Berkshire, England.
22. Hashin, Z., "Failure Criteria for Unidirectional Fiber Composites," Journal of Applied Mechanics, Vol. 47, June 1980.

Table 1. Ply Properties (T300/5208, V_f = .7)

E_1	=	153.0 GPa
E_2	=	10.9 GPa
ν_{12}	=	.3
G_{12}	=	5.6 GPa
G_{13}	=	5.6 GPa
G_{23}	=	4.2 GPa
ρ	=	1.55 g/cc
t	=	.0132 cm

Ply Strengths

S_{1C}	=	758 MPa
S_{1T}	=	689 MPa
S_{2C}	=	96.5 MPa
S_{2T}	=	27.6 MPa
S_{12}	=	62 MPa
S_{13}	=	62 MPa
S_{23}	=	62 MPa
S_{IF}	=	62 MPa

Table 2. Impactor and Contact Spring Parameters

Impactor Mass = 16.45 g (1.59 cm dia. steel ball)

Initial Velocity = -9.4 m/s

Initial Position = 0.0

Spring constant (K) = 6.55×10^8 (N/m^n)

Loading exponent (n) = 1.5

Unloading exponent (m) = 2.5

Indentation constant (c) = 6.067×10^4 (m^{1-i})

Indentation exponent (i) = 2.4

Table 3. Damage Summary

Time (μsec)	Element	Ply	Mode
35	90	1	Fiber
	90	2	Matrix
	91	1	Matrix
	102	1	Matrix
	103	1	Fiber
	103	2	Matrix
40°	90	3	Matrix
	103	3	Matrix
45	90	8	Fiber
	103	8	Fiber
70	91	2	Matrix
	102	2	Matrix
80	78	2	Matrix
	115	2	Matrix
90	79	1	Matrix
	114	1	Matrix
100	79	2	Matrix
	114	2	Matrix

Table 4. Cumulative Damage After 100 μsec

Ply	Elements with Matrix Damage	Elements with Fiber Damage
1	79,91,102,114	90,103
2	78,79,90,91, 102,103,114, 115	--
3	90,103	--
4	--	--
5	--	--
6	--	--
7	--	--
8	--	90,103

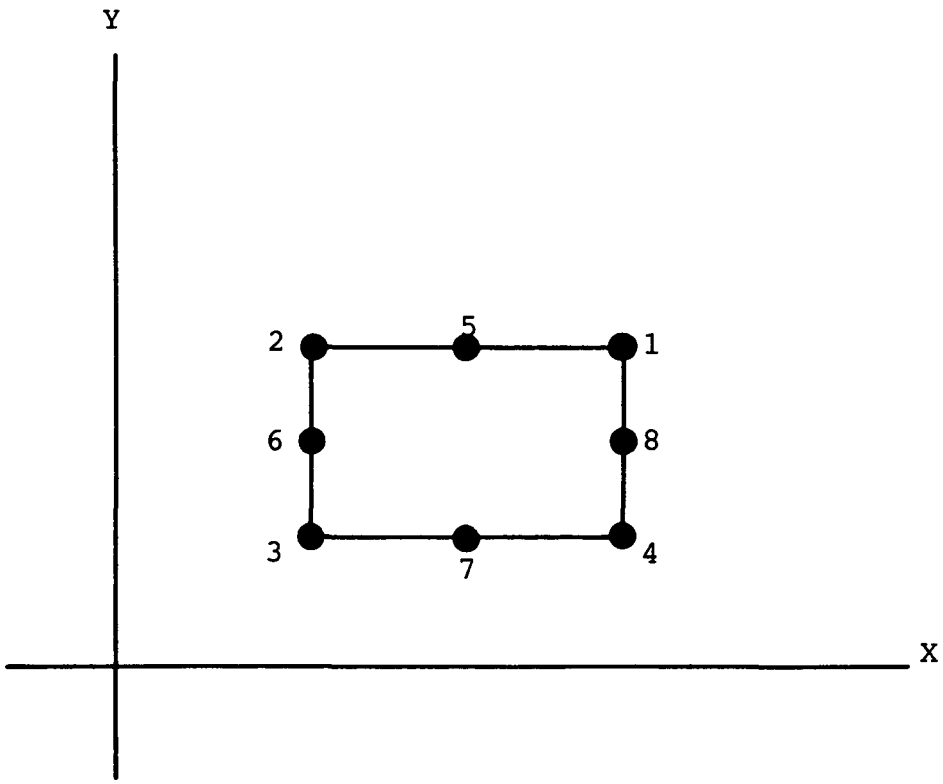

Figure 1. Element Orientation Required for Incorporating Delaminations

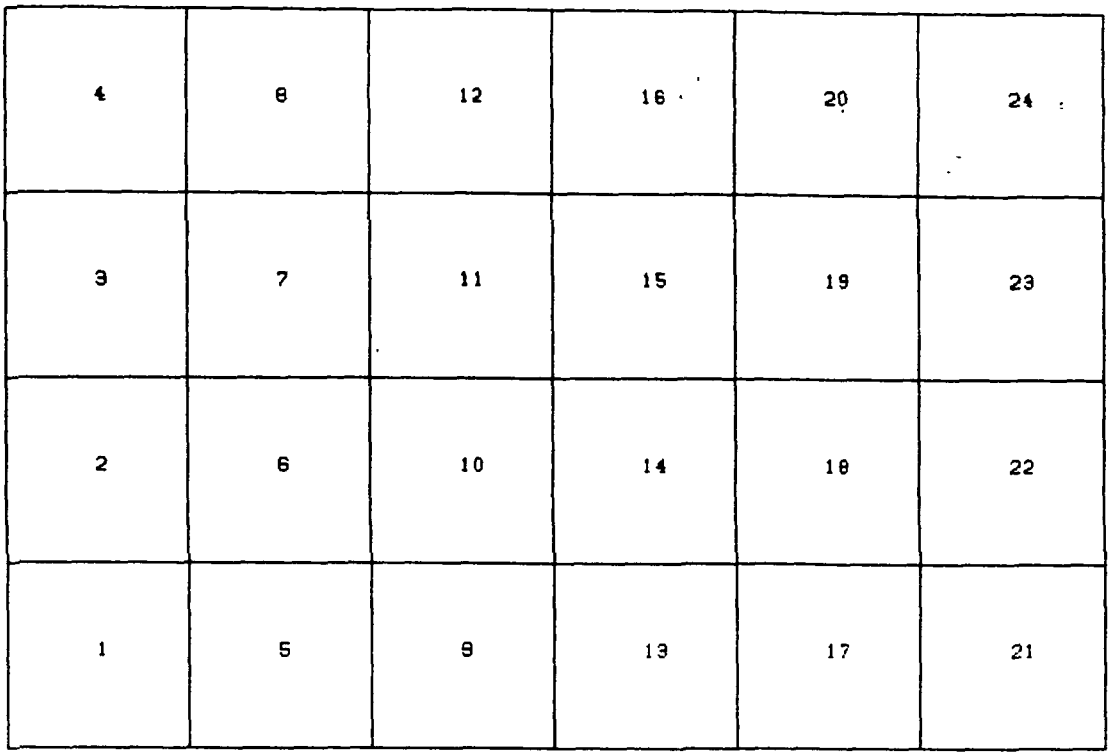

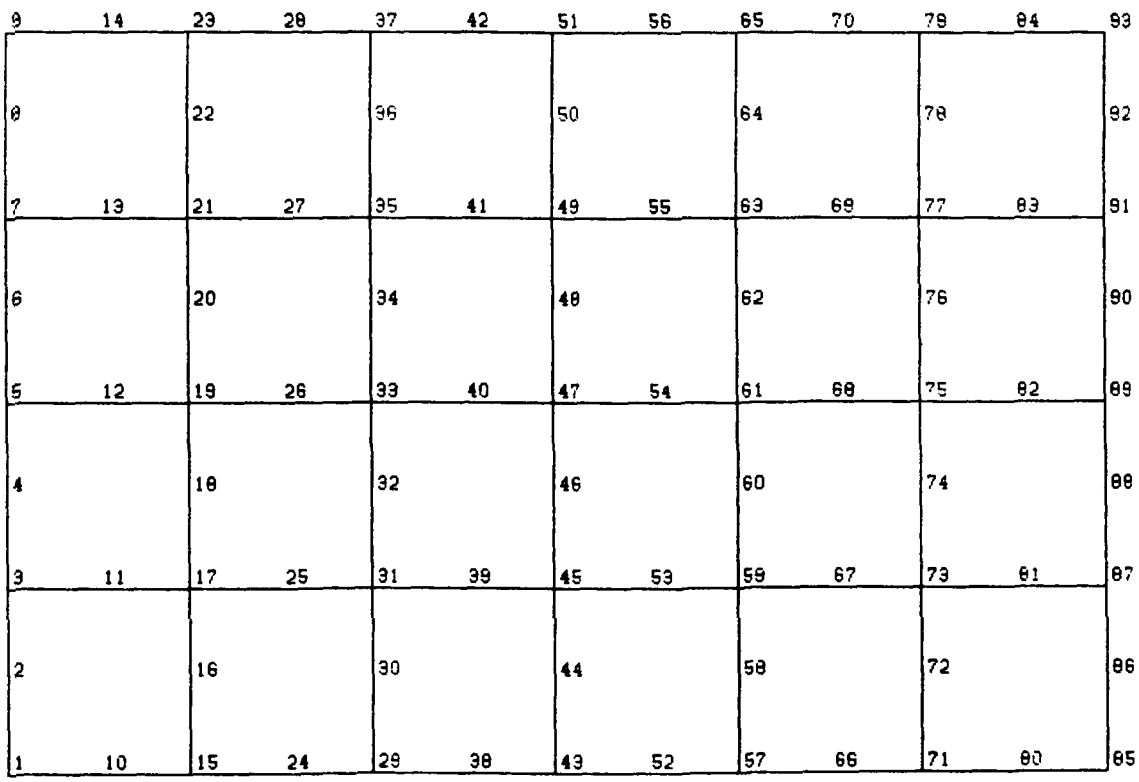

Figure 2. Coarse Finite Element Mesh

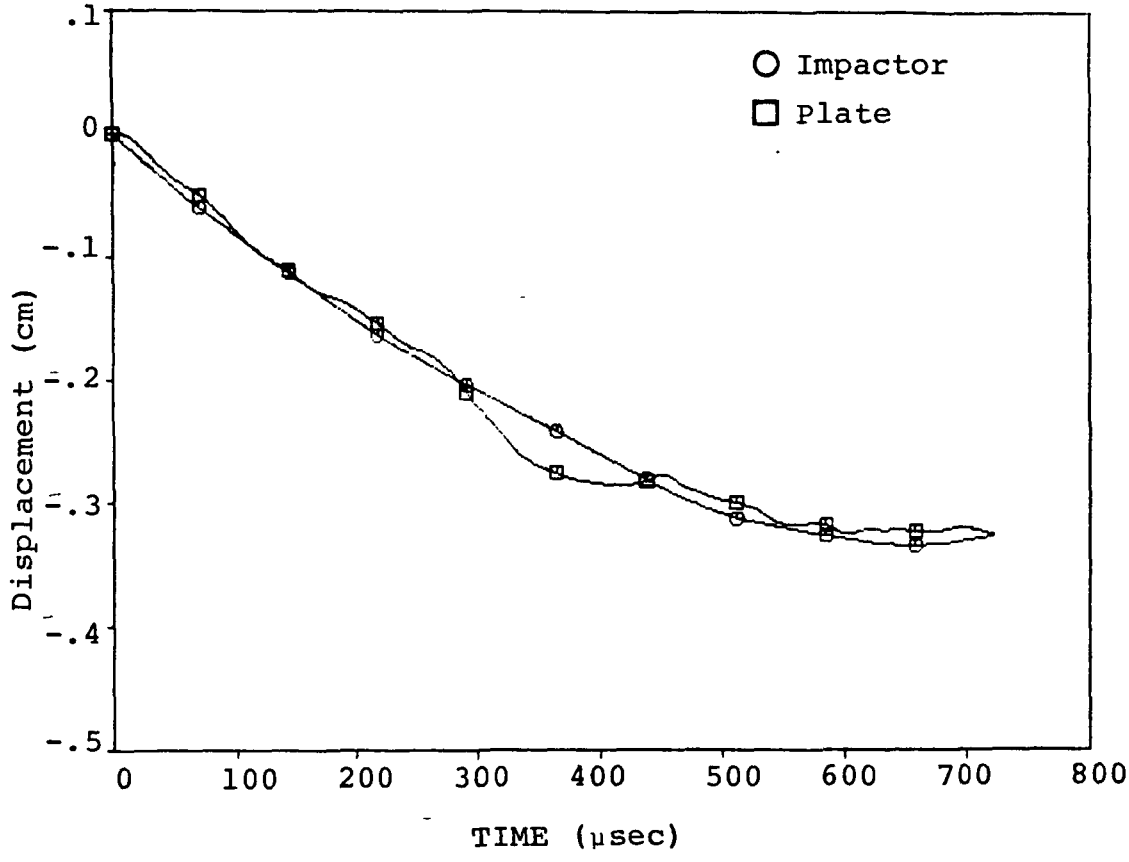

Figure 3. Time History of the Impactor and Impacted Node

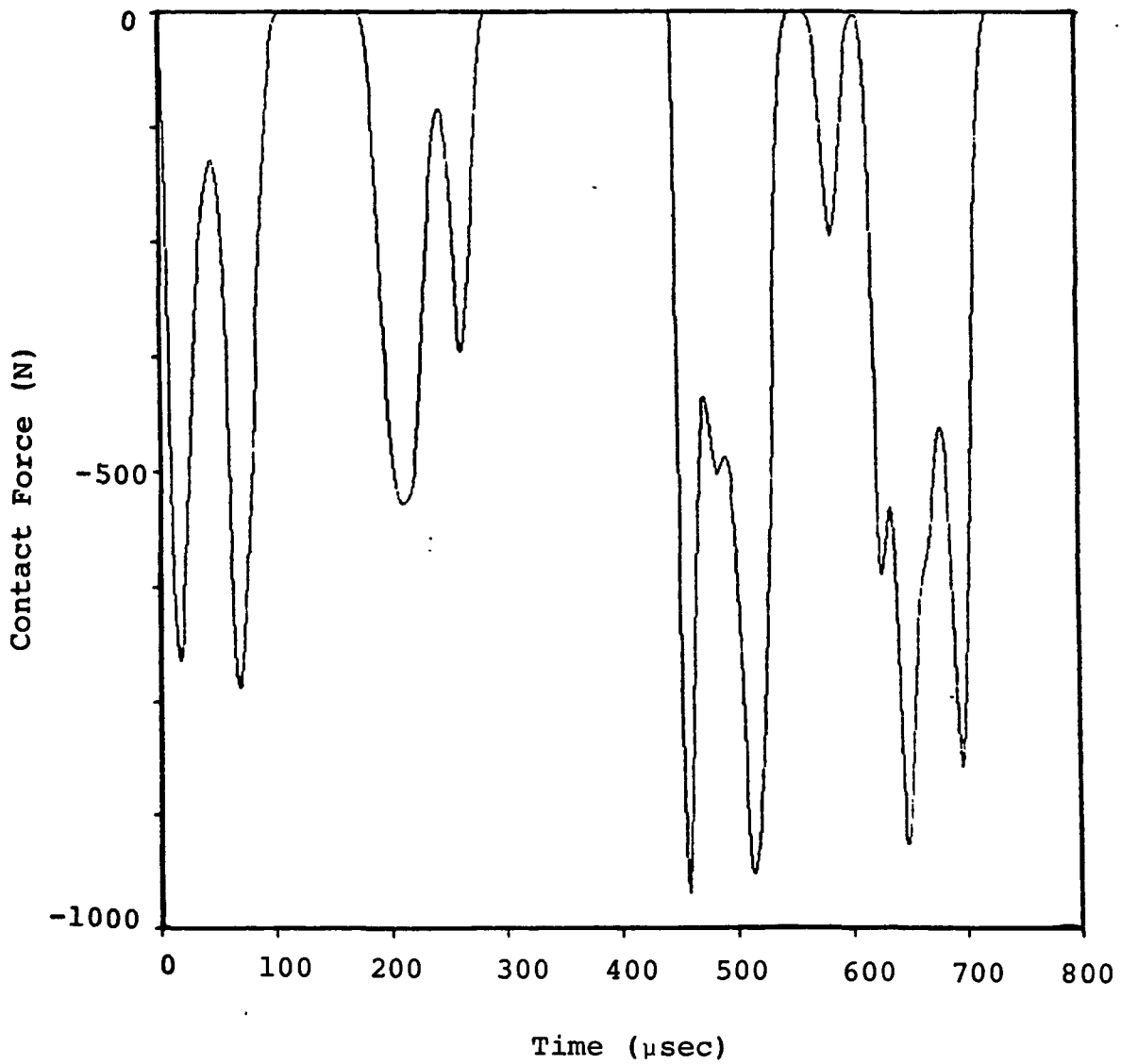

Figure 4. Contact Force vs. Time

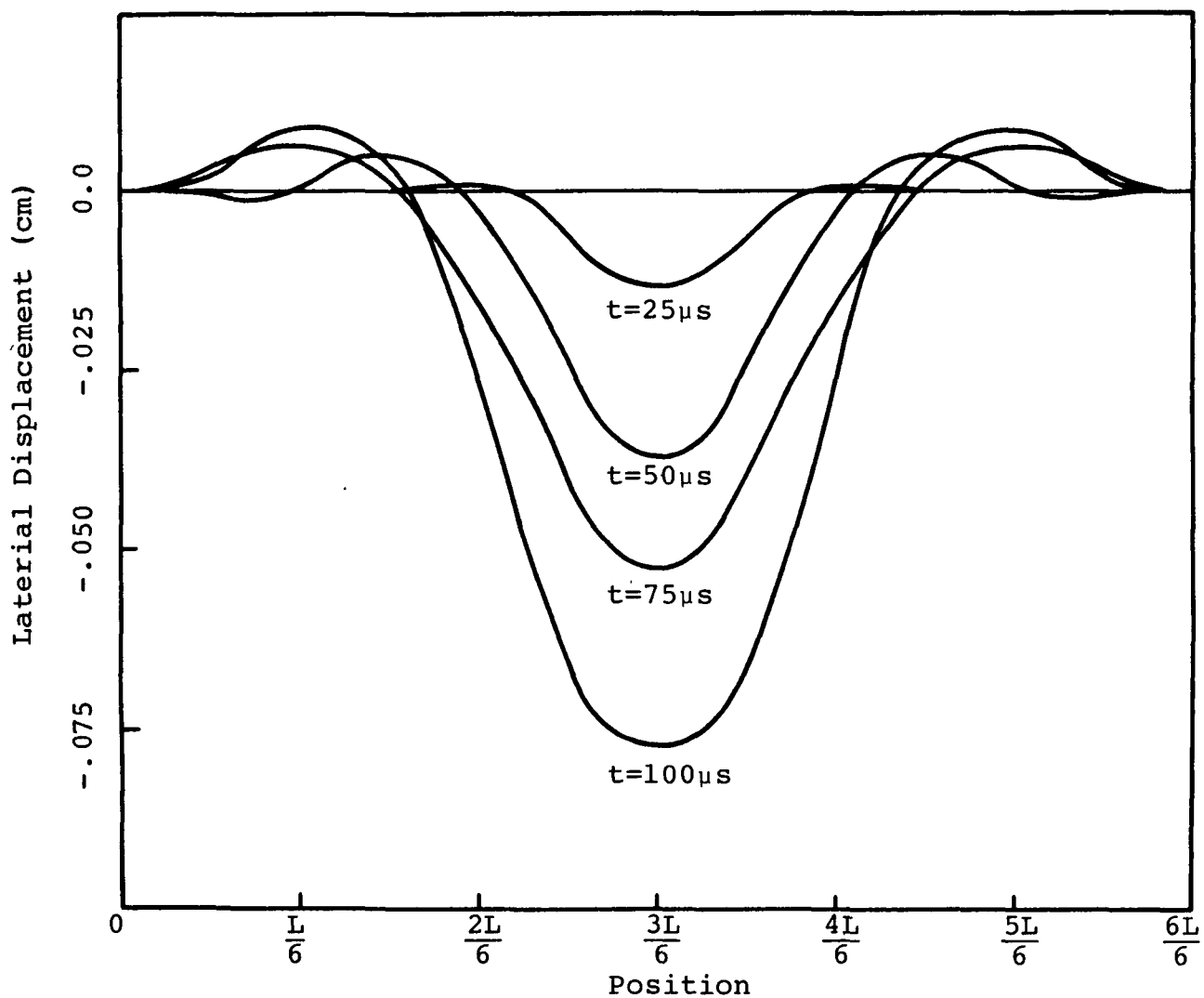

Figure 5. Lateral Displacement of the Major Chord

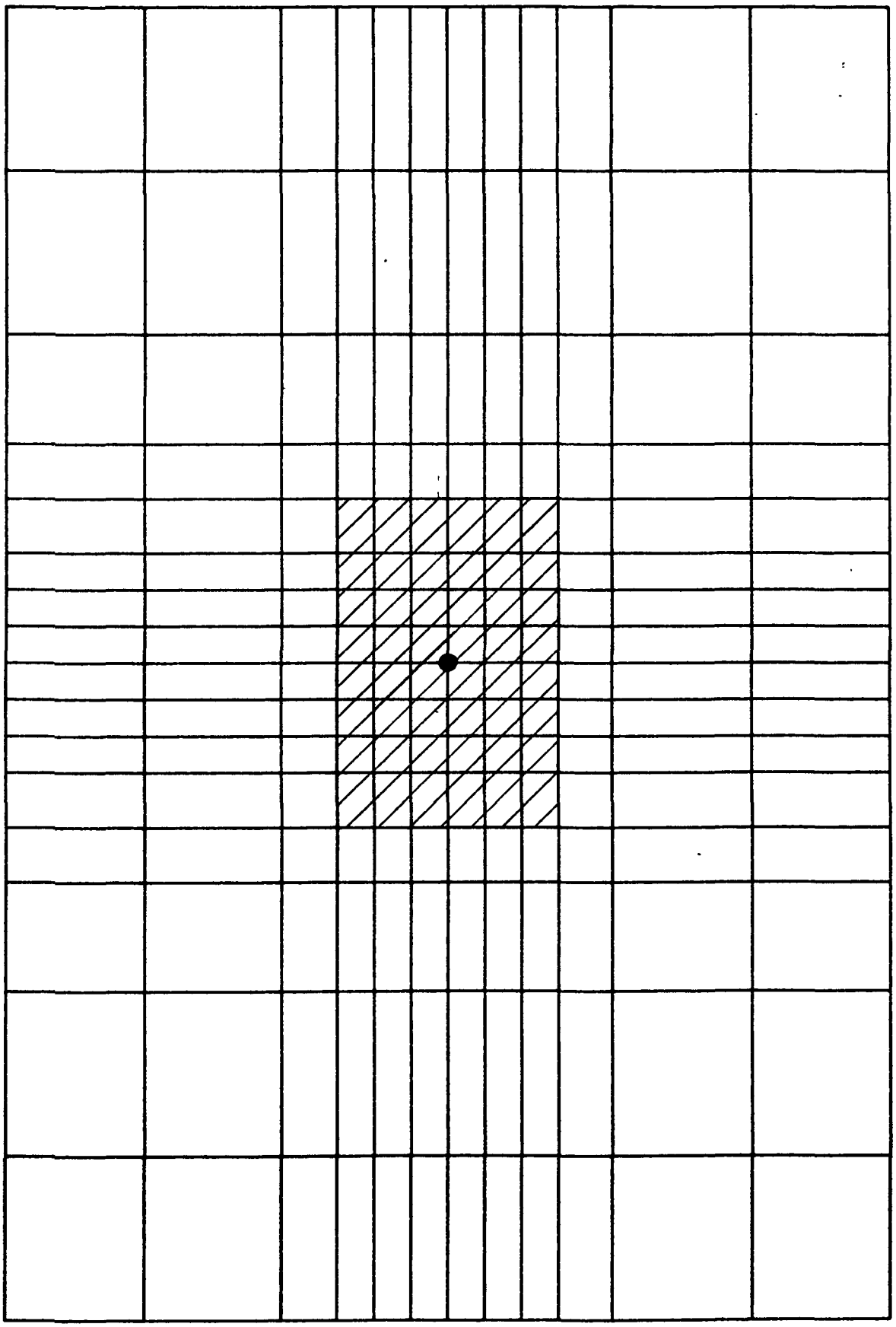

Figure 6. Finite Element Mesh for the Second Analysis

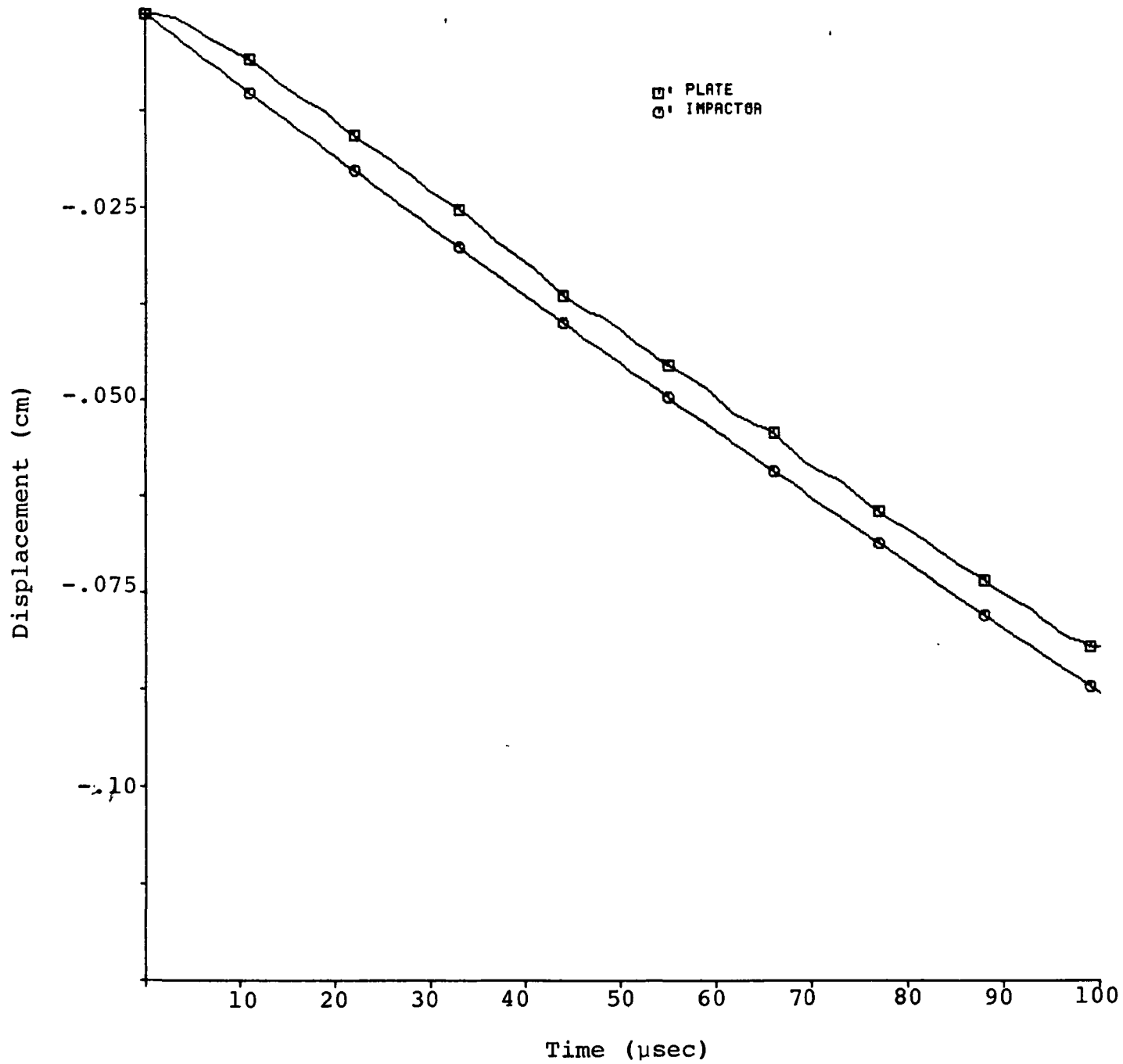

Figure 7. Lateral Deflection of the Plate and Impactor

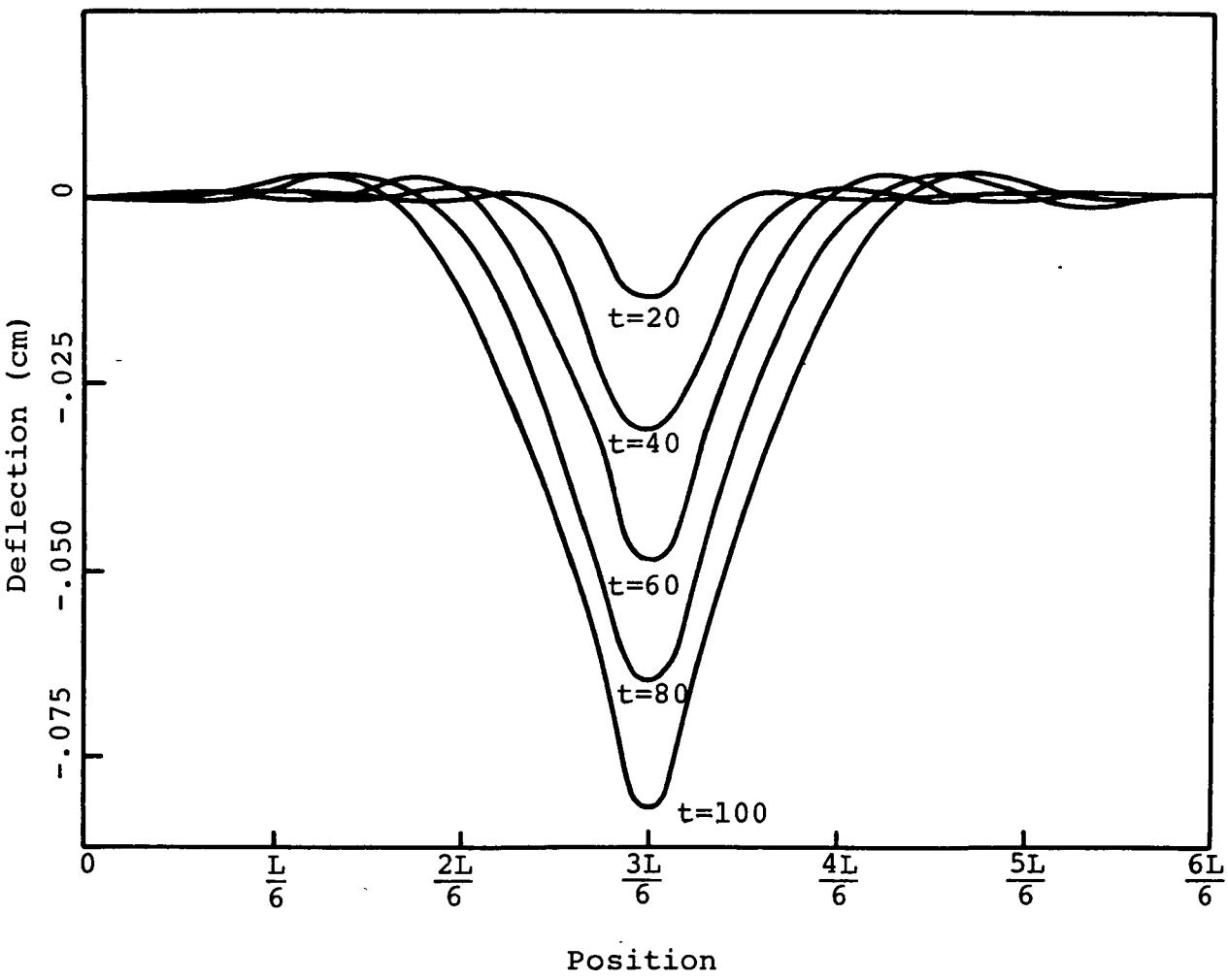

Figure 8. Lateral Deflection of the Major Chord

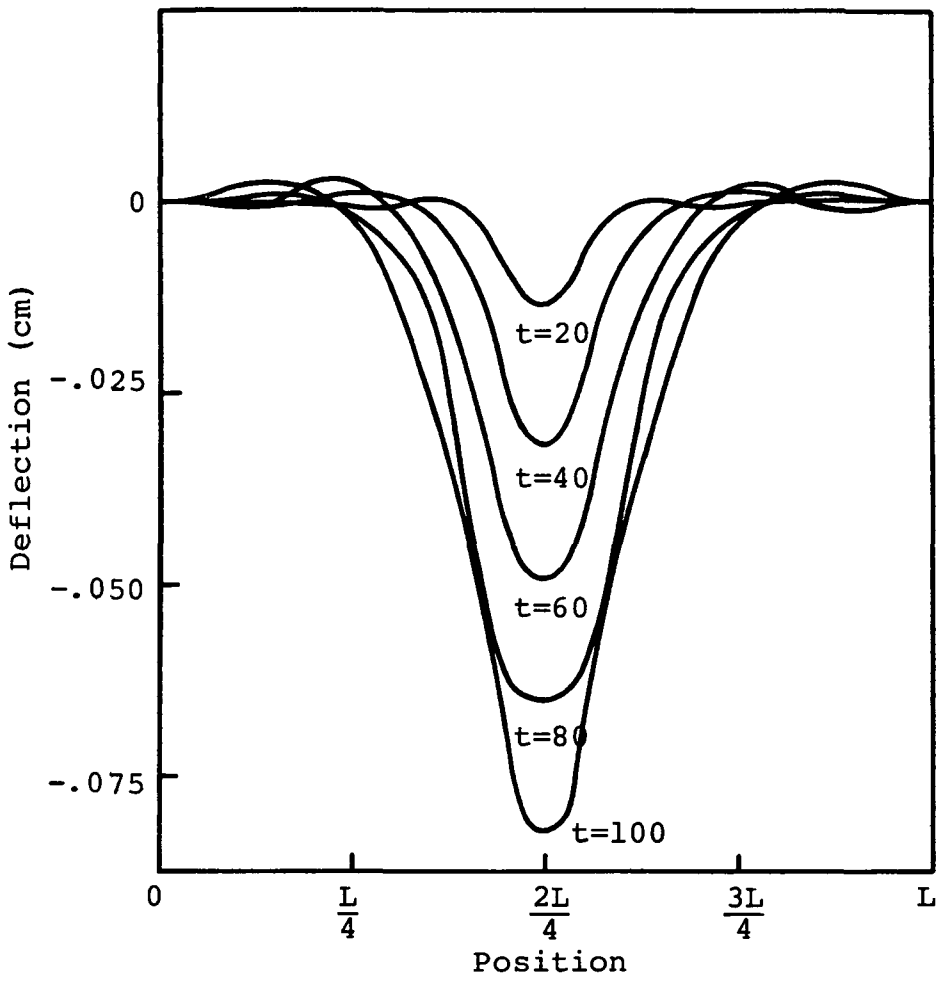

Figure 9. Lateral Deflection of the Minor Chord

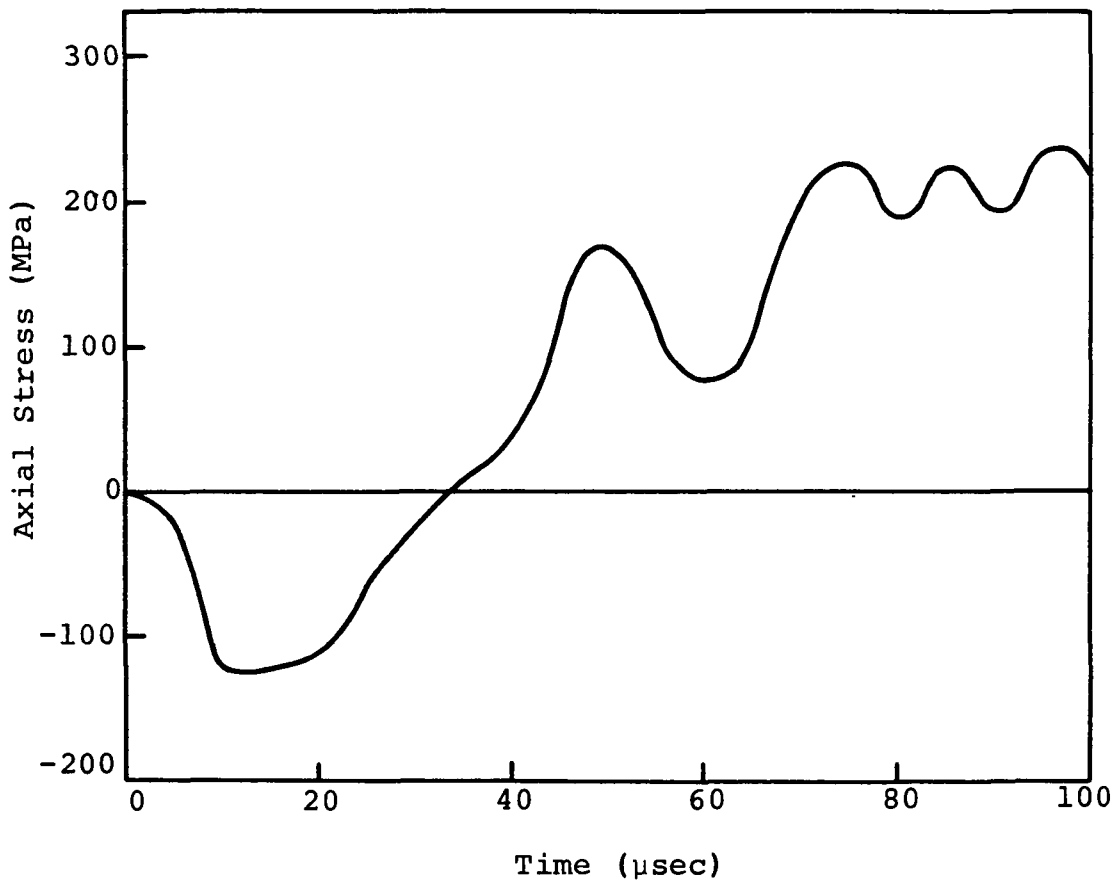

Figure 10. Fiber Direction Stress in the Bottom 45° Ply of Element 79

181	169	157	145	133	121	109	97	85	73	61	49	37	25	13	1
182	170	158	146	134	122	110	98	86	74	62	50	38	26	14	2
183	171	159	147	135	123	111	99	87	75	63	51	39	27	15	3
184	172	160	148	136	124	112	100	88	76	64	52	40	28	16	4
185	173	161	149	137	125	113	101	89	77	65	53	41	29	17	5
186	174	162	150	138	126	114	102	90	78	66	54	42	30	18	6
187	175	163	151	139	127	115	103	91	79	67	55	43	31	19	7
188	176	164	152	140	128	116	104	92	80	68	56	44	32	20	8
189	177	165	153	141	129	117	105	93	81	69	57	45	33	21	9
190	178	166	154	142	130	118	106	94	82	70	58	46	34	22	10
191	179	167	155	143	131	119	107	95	83	71	59	47	35	23	11
192	180	168	156	144	132	120	108	96	84	72	60	48	36	24	12

Figure 11. Element Numbers for Refined Mesh

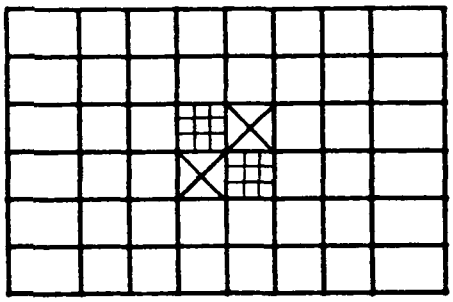

35 μsec ply 1

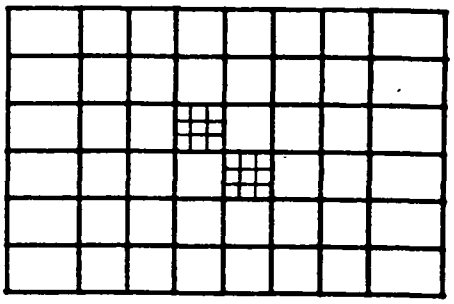

70 μsec ply 2

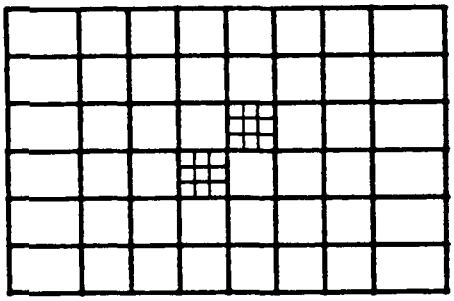

35 μsec ply 2

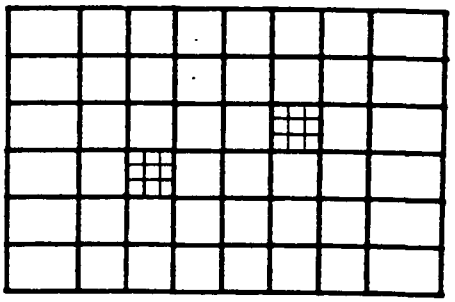

80 μsec ply 2

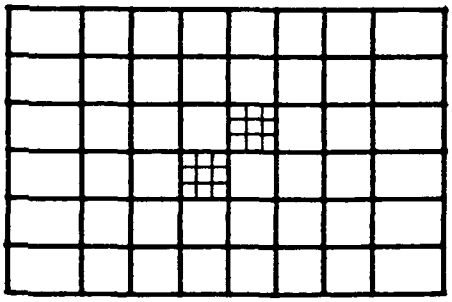

40 μsec ply 3

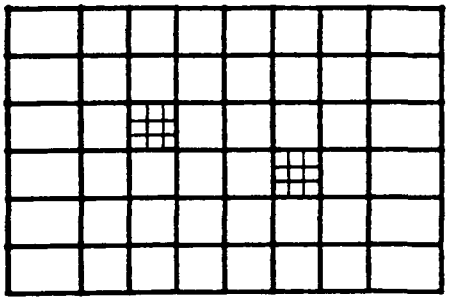

90 μsec ply 1

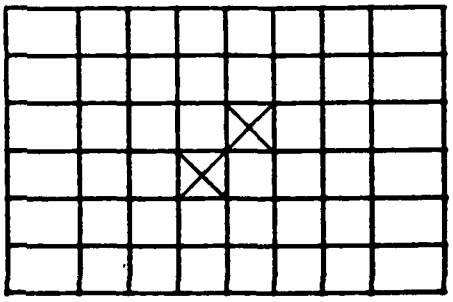

45 μsec ply 8

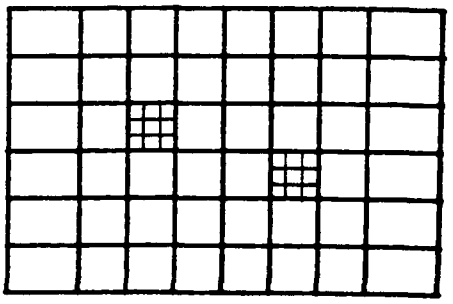

100 μsec ply 2

Fiber Failure

Matrix Failure

Figure 12. Damage Progression during 100 μsec of Impact Event $[45/0/-45/90]_S$ T300/5208 Laminate Impacted by a 1.59 Diameter Steel Sphere at 9.4 m/sec. Ply 1 is Opposite Impact Point

APPENDIX A

THE ISOPARAMETRIC THICK SHELL ELEMENT

The element used in CLIP II is an extension of the eight noded isoparametric plate bending element with shear deformation developed by Hinton et. al (ref. 19). Membrane effects and bending-extensional coupling have been added to the basic element presented in reference 19, resulting in an element well suited for the study of composite plates.

Although the Kirchoff hypothesis that lines originally normal to the plate remain normal after deformation is not used, other assumptions have been made. They are:

1. Lateral displacements are small.
2. Lines originally normal to the plate remain straight.
3. Normal strains and stresses are negligible.

Shear deformation has been included in this element by allowing the rotations of the normal about the global x and y axes, and the lateral plate displacement to very independently. By assuming a linear variation of u and v with respect to the z axis (assumption 2), the element may be integrated explicitly through the thickness, reducing the three dimensional problem to two dimensions.

While it is known that normals do not stay straight during deformation, the rotations about the coordinate axes may be thought of as average values, and the actual nonuniform through-the-thickness shear distribution accounted for by an alternate procedure.

The displacement field for this element is given by:

$$u(x,y,z) = u_o(x,y)+z\theta_x(x,y) \tag{A.1}$$

$$v(x,y,z) = v_o(x,y)-z\theta_y(x,y) \tag{A.2}$$

$$w(x,y,z) = w_o(x,y) \tag{A.3}$$

where u_o, v_o and w_o are the displacements of the mid-plane, and θ_x and θ_y are the rotations in the x-z and y-z planes, as shown in figures A.1 and A.2.

Using this displacement field and assumptions 1 and 3, the strains are given by

$$\{\bar{\varepsilon}\} = \begin{Bmatrix} \varepsilon_x \\ \varepsilon_y \\ \gamma_{xy} \\ \gamma_{xz} \\ \gamma_{yz} \end{Bmatrix} = \begin{bmatrix} \frac{\partial}{\partial x} & 0 & 0 & z\frac{\partial}{\partial x} & 0 \\ 0 & \frac{\partial}{\partial y} & 0 & 0 & -z\frac{\partial}{\partial y} \\ \frac{\partial}{\partial y} & \frac{\partial}{\partial x} & 0 & z\frac{\partial}{\partial y} & -z\frac{\partial}{\partial x} \\ 0 & 0 & \frac{\partial}{\partial x} & +1 & 0 \\ 0 & 0 & \frac{\partial}{\partial y} & 0 & -1 \end{bmatrix} \begin{Bmatrix} u_o \\ v_o \\ w_o \\ \theta_y \\ \theta_x \end{Bmatrix} \qquad (A.4)$$

These strains may be separated into two parts, one accounting for membrane strains and the other for bending strains.

$$\{\bar{\varepsilon}\} = \{\bar{\varepsilon}_M\} + \{\bar{\varepsilon}_B\} = [\bar{B}_M]\{\bar{u}\} + [B_B]\{\bar{u}\} \qquad (A.5)$$

where

$$[\bar{B}_M] = \begin{bmatrix} \frac{\partial}{\partial x} & 0 & 0 & 0 & 0 \\ 0 & \frac{\partial}{\partial y} & 0 & 0 & 0 \\ \frac{\partial}{\partial y} & \frac{\partial}{\partial x} & 0 & 0 & 0 \\ 0 & 0 & 0 & 0 & 0 \\ 0 & 0 & 0 & 0 & 0 \end{bmatrix} \qquad (A.6)$$

$$[\bar{B}_B] = \begin{bmatrix} 0 & 0 & 0 & +z\frac{\partial}{\partial x} & 0 \\ 0 & 0 & 0 & 0 & -z\frac{\partial}{\partial y} \\ 0 & 0 & 0 & +z\frac{\partial}{\partial y} & -z\frac{\partial}{\partial x} \\ 0 & 0 & \frac{\partial}{\partial x} & +1 & 0 \\ 0 & 0 & \frac{\partial}{\partial y} & 0 & -1 \end{bmatrix} \qquad (A.7)$$

and

$$\{\bar{u}\}^T = \{u_o(x,y) \quad v_o(x,y) \quad w_o(x,y) \quad \theta_x(x,y) \quad \theta_y(x,y)\} \qquad (A.8)$$

The displacement field is approximated with parabolic shape functions, using the displacements and rotations at the eight nodes shown in figure A.2. To aid in itegrating over the area of the element, the original element geometry is mapped onto a two unit square in an r-s coordinate system, as shown in figure A.2. Being isoparametric, this coordinate mapping is done with the same functions used to approximate the displacement field. These functions are of the serindipity type, and have the form

$$h_i = \frac{1}{4} \cdot (1+r_i r) \cdot (1+s_i s) \cdot (r_i r + s_i s - 1) \qquad i=1,2,3,4 \qquad (A.9)$$

and

$$h_i = \frac{1}{2} \cdot (1+r_i r) \cdot (1+s_i s) \cdot (1-r_i{}^2 r^2) \cdot (1-s_i{}^2 s^2) \qquad i=5,6,7,8 \qquad (A.10)$$

Using these shape functions, any function of r and s may be approximated by

$$f(r,s) = \sum_{i=1}^{8} h_i f_i \qquad (A.11)$$

Further, partial derivatives with respect to r and s are given by

$$\frac{\partial f}{\partial r} = \sum_{i=1}^{8} \frac{\partial h_i}{\partial r} f_i \tag{A.12}$$

$$\frac{\partial f}{\partial s} = \sum_{i=1}^{8} \frac{\partial h_i}{\partial s} f_i \tag{A.13}$$

Since strains have been defined in terms of the derivatives with respect to x and y, a coordinate transformation for the derivatives is needed. This transformation is found by applying the chain rule for derivatives.

$$\begin{Bmatrix} \frac{\partial}{\partial r} \\ \frac{\partial}{\partial s} \end{Bmatrix} = \begin{bmatrix} \frac{\partial x}{\partial r} & \frac{\partial y}{\partial r} \\ \frac{\partial x}{\partial s} & \frac{\partial y}{\partial s} \end{bmatrix} \begin{Bmatrix} \frac{\partial}{\partial x} \\ \frac{\partial}{\partial y} \end{Bmatrix} = [J] \begin{Bmatrix} \frac{\partial}{\partial x} \\ \frac{\partial}{\partial y} \end{Bmatrix} \tag{A.14}$$

The Jacobian transformation matrix [J] is evaluated with the aid of (A.12) and (A.13).

$$[J] = \begin{bmatrix} \frac{\partial h_1}{\partial r} & \frac{\partial h_2}{\partial r} & \cdots & \frac{\partial h_8}{\partial r} \\ \frac{\partial h_1}{\partial s} & \frac{\partial h_2}{\partial s} & \cdots & \frac{\partial h_8}{\partial s} \end{bmatrix} \begin{bmatrix} x_1 & y_1 \\ x_2 & y_2 \\ \cdot & \cdot \\ \cdot & \cdot \\ \cdot & \cdot \\ x_8 & y_8 \end{bmatrix} \tag{A.15}$$

Partial derivatives with respect to x and y are then given by inverting (A.14) and substituting (A.12) and (A.13).

$$\begin{Bmatrix} \frac{\partial f}{\partial x} \\ \frac{\partial f}{\partial y} \end{Bmatrix} = [J]^{-1} \begin{bmatrix} \frac{\partial h_1}{\partial r} & \frac{\partial h_2}{\partial r} & \cdots & \frac{\partial h_8}{\partial r} \\ \frac{\partial h_1}{\partial s} & \frac{\partial h_2}{\partial s} & \cdots & \frac{\partial h_8}{\partial s} \end{bmatrix} \begin{Bmatrix} f_1 \\ f_2 \\ \vdots \\ f_8 \end{Bmatrix} = [P] \{\bar{f}\} \tag{A.16}$$

The strain-displacement relationship for the element is now obtained by substituting (A.16) into (A.6) and (A.7).

$$\{\bar{\varepsilon}\} = \left([B_M] + [B_B]\right) \{u\} \tag{A.17}$$

with

$$\{u\}^T = \left\{u_{o_1} \; v_{o_1} \; w_{o_1} \; \theta_{x_1} \; \theta_{y_1} \; \cdots \; u_{o_8} \; v_{o_8} \; w_{o_8} \; \theta_{x_8} \; \theta_{y_8}\right\} \tag{A.18}$$

$$[B_M] = \begin{bmatrix} p_{11} & 0 & 0 & 0 & 0 & p_{12} & 0 & 0 & 0 & 0 & \cdots & p_{18} & 0 & 0 & 0 & 0 \\ 0 & p_{21} & 0 & 0 & 0 & 0 & p_{22} & 0 & 0 & 0 & \cdots & 0 & p_{28} & 0 & 0 & 0 \\ p_{21} & p_{11} & 0 & 0 & 0 & p_{22} & p_{12} & 0 & 0 & 0 & \cdots & p_{28} & p_{18} & 0 & 0 & 0 \\ 0 & 0 & 0 & 0 & 0 & 0 & 0 & 0 & 0 & 0 & \cdots & 0 & 0 & 0 & 0 & 0 \end{bmatrix} \tag{A.19}$$

and

$$[B_B] = \begin{bmatrix} 0\ 0\ 0 & zp_{11} & 0 & 0\ 0\ 0 & zp_{12} & 0 & \cdots & 0\ 0\ 0 & zp_{18} & 0 \\ 0\ 0\ 0 & 0 & -zp_{21} & 0\ 0\ 0 & 0 & -zp_{22} & \cdots & 0\ 0\ 0 & 0 & -zp_{28} \\ 0\ 0\ 0 & zp_{21} & -zp_{11} & 0\ 0\ 0 & zp_{22} & -zp_{12} & \cdots & 0\ 0\ 0 & zp_{28} & -zp_{18} \\ 0\ 0 & p_{11} & +1 & 0\ 0 & p_{12} & +1 & 0 & \cdots & 0\ 0 & p_{18} & +1 & 0 \\ 0\ 0 & p_{21} & 0 & -1 & 0\ 0 & p_{22} & 0 & -1 & \cdots & 0\ 0 & p_{28} & 0 & -1 \end{bmatrix} \qquad (A.20)$$

where p_{ij} is the ij^{th} element of the matrix [P] defined by (A.16).

Using standard finite element techniques, see references 20 and 21, the stiffness matrix for this element may be calculated from

$$[K] = \int^{vol} [B]^T [D] [B] dv \qquad (A.21)$$

where [D] is the 5x5 stress-strain relationship defined by

$$\{\bar{\sigma}\} = [D]\{\bar{\varepsilon}\} \qquad (A.22)$$

where

$$\{\bar{\sigma}\}^T = \{\sigma_x \sigma_y \tau_{xy} \tau_{xz} \tau_{yz}\} \qquad (A.23)$$

and

$$\{\bar{\varepsilon}\}^T = \{\varepsilon_x \varepsilon_y \gamma_{xy} \gamma_{xz} \gamma_{yz}\} \qquad (A.24)$$

Since the matrix [B] is the sum of two matrices, the integral in (A.21) may be rewritten as

$$[K] = \int^{vol} [B_M]^T [D] [B_M] dv + \int^{vol} [B_M]^T [D] [B_B] dv + \int^{vol} [B_B]^T [D] [B_M] dv + \int^{vol} [B_B]^T [D] [B_B] dv \qquad (A.25)$$

The total element stiffness matrix may then be thought of as the sum of four stiffness matrices

$$[K] = [K_1] + [K_2] + [K_3] + [K_4] \tag{A.26}$$

considering the first of these four matrices

$$[K_1] = \int^{vol} [B_M]^T [D] [B_M] dv \tag{A.27}$$

From (A.19), it can be seen that the matrix $[B_M]$ is independent of z, allowing (A.26) to be rewritten as

$$[K_1] = t\int^{area} [B_M]^T [D] [B_M] dA \tag{A.28}$$

This matrix is recognized as the plane stress stiffness matrix, and includes only in-plane effects. The upper 3x3 of [D] is the only portion of this matrix that is utilized, and is recognized as the [A] matrix from laminated plate theory, when multiplied by t.

The matrics $[K_2]$ and $[K_3]$ are considered together, since it can be shown that

$$[K_2] = [K_3]^T \tag{A.29}$$

The expression for $[B_B]$, given by (A.20), may be expressed as the product of two matrices

$$[B_B] = [Z] [B_B^*] \tag{A.30}$$

where

$$[Z] = \begin{bmatrix} z & 0 & 0 & 0 & 0 \\ 0 & z & 0 & 0 & 0 \\ 0 & 0 & z & 0 & 0 \\ 0 & 0 & 0 & 1 & 0 \\ 0 & 0 & 0 & 0 & 1 \end{bmatrix} \tag{A.31}$$

and

$$[B_B^*] = \begin{bmatrix} 0\ 0\ 0 & P_{11} & 0 & 0\ 0\ 0 & P_{21} & 0 & \cdots & 0\ 0\ 0 & P_{18} & 0 \\ 0\ 0\ 0 & 0 & -P_{21} & 0\ 0\ 0 & 0 & -P_{22} & \cdots & 0\ 0\ 0 & 0 & -P_{28} \\ 0\ 0\ 0 & P_{21} & -P_{11} & 0\ 0\ 0 & P_{22} & -P_{21} & \cdots & 0\ 0\ 0 & P_{28} & -P_{18} \\ 0\ 0\ P_{11} & 1 & 0 & 0\ 0\ P_{21} & 1 & 0 & \cdots & 0\ 0\ P_{18} & 1 & 0 \\ 0\ 0\ P_{21} & 0 & -1 & 0\ 0\ P_{22} & 0 & -1 & \cdots & 0\ 0\ P_{28} & 0 & -1 \end{bmatrix} \tag{A.32}$$

This allows the expression for $[K_2]$ to be written as

$$[K_2] = \int^{area} [B_B^*]^T \left(\int_{-t/2}^{t/2} [Z][D]dz \right) [B_M]dA \tag{A.33}$$

The innermost integral of (A.33) may be evaluated explicitly, and represents bending-extensional coupling. The upper 3x3 of the resulting integration is the [B] matrix from laminated plate theory. For homogeneous isotropic materials or balanced symmetric laminates, this integral will vanish.

The expression for $[B_B]$ given by (A.30) is also utilized to evaluate $[K_4]$. Substituting this expresison yields

$$[K_4] = \int^{area} [B_B^*]^T \left(\int_{-t/2}^{t/2} [Z]^T[D][Z]dz \right) [B_B^*]dA \tag{A.34}$$

Again, the innermost integral of (A.34) may be evaluated explicitly. This integral represents the bending properties of the element, and may give rise to bending-twisting coupling, depending on the nature of [D]. The upper 3x3 of this matrix is the [D] matrix from laminated plate theory, the lower right 2x2 submatrix of [D] contains the shear terms. It is this submatrix which must be corrected to account for nonuniform shear distributions in the z direction. For homogeneous isotropic plates, the shear distribution is known to be parabolic, resulting in a correction factor of 5Gt/6. For laminates, however, the shear distribution is not so well defined, requiring that more complicated procedures be used.

The procedure used in CLIP II is based on the method developed by Cohen in reference 19. Cohen presents a method for determining the constitutive equation for transverse shear without specifying a priori the through-the-thickness distribution. This method involves the application of Castigliano's theorem to minimize the shear strain energy, which is defined in terms of a Taylor series containing arbitrary constants. The details of this procedure are beyond the scope of this report, but can be found in reference 19.

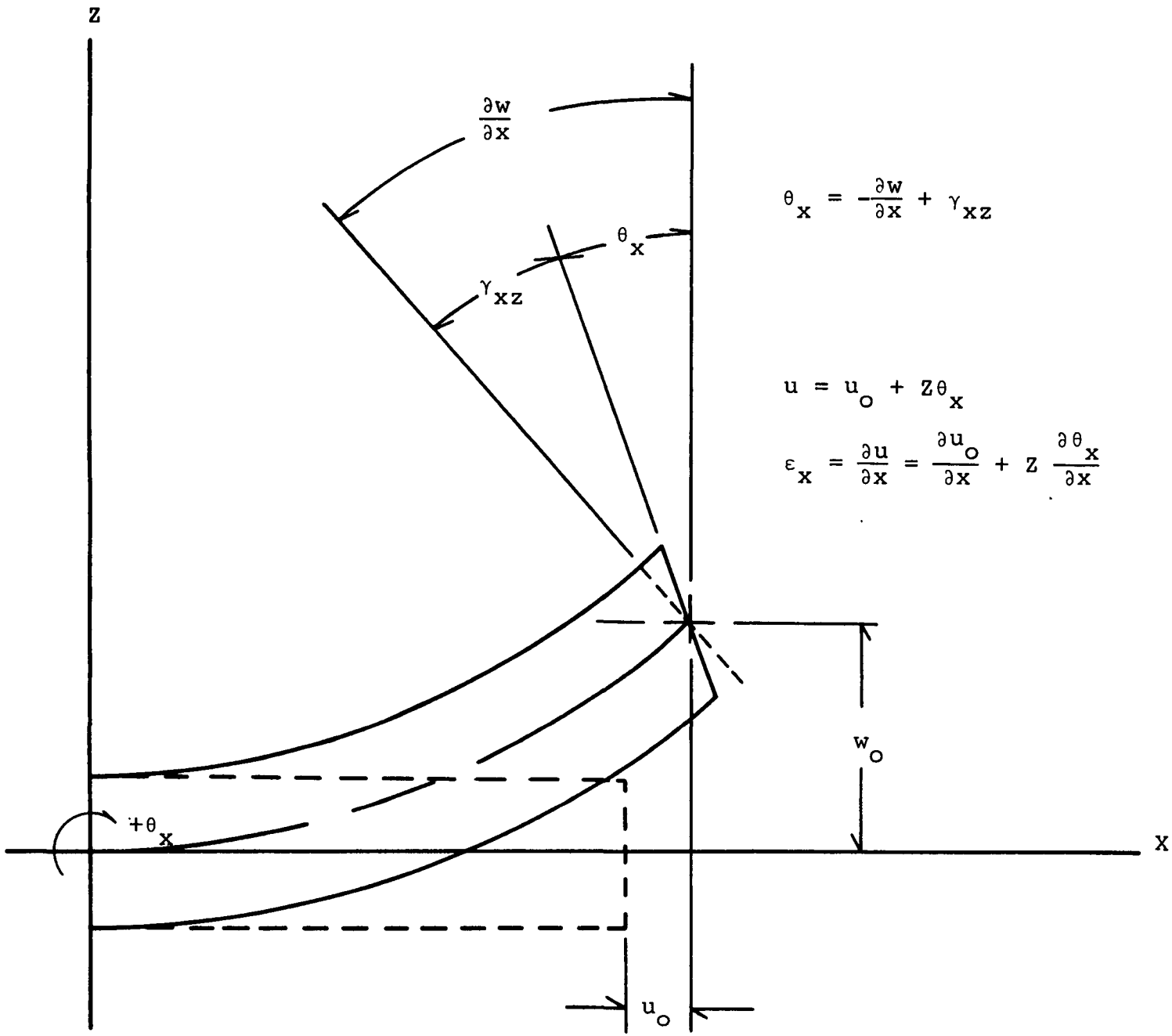

Figure A.1. Extensional Strain in the X Direction

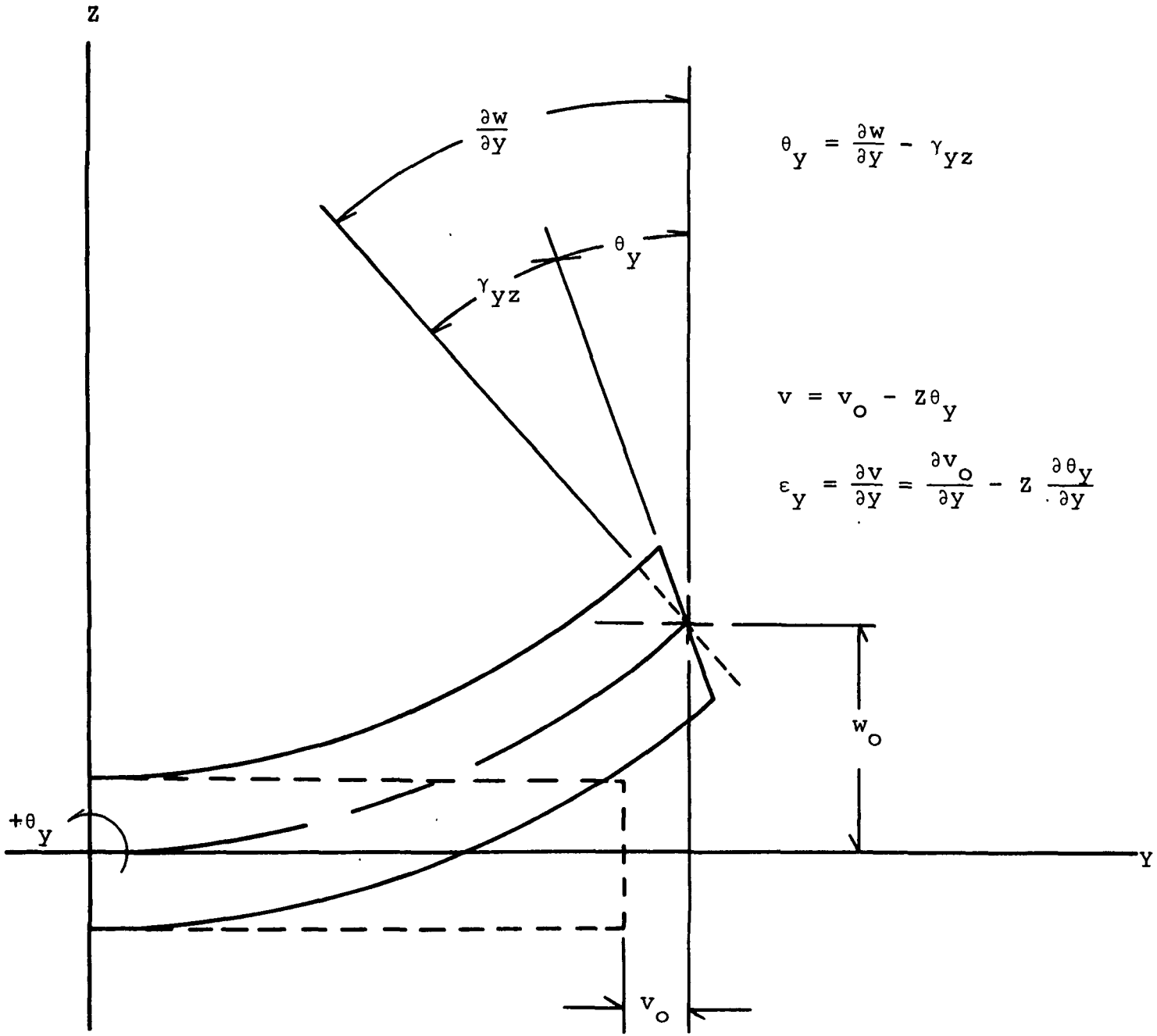

Figure A.2. Extensional Strain in the Y Direction

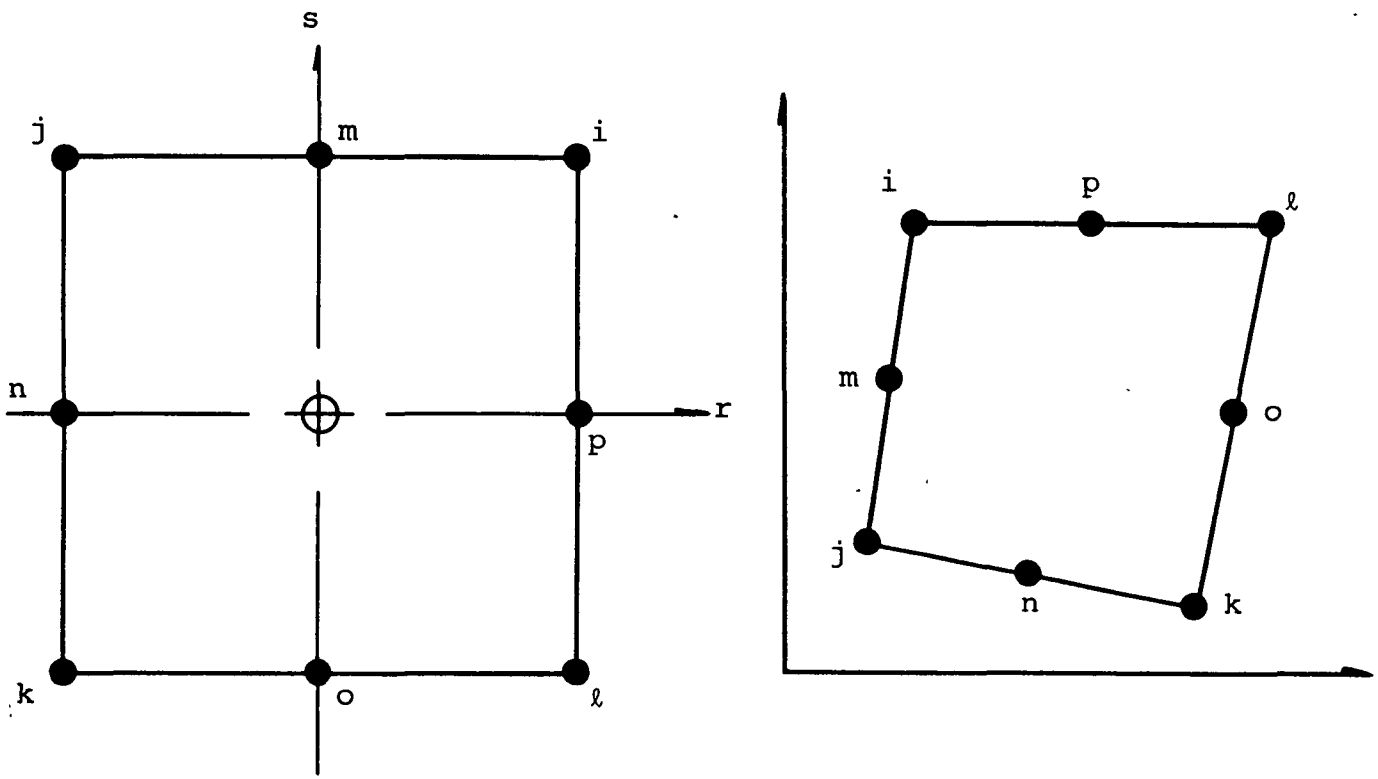

Figure A.3. Mapping Distorted Shapes in the r-s Coordinate

APPENDIX B
THE NONLINEAR CONTACT SPRING

CLIP II models the impactor as a lumped mass which is tied to the plate at a single node by a nonlinear spring. This spring contains hysterisis, and has the ability to vanish if the plate and impactor have separated. The general force-displacement relationship for this spring were determined by Sun and Yang (refs. 16 and 17) and are

$$F = K\delta^n \tag{B.1}$$

if the spring is loading, and by

$$F = F_{max}\left(\frac{\delta-\delta_o}{\delta_{max}-\delta_o}\right)^m \tag{B.2}$$

if the spring is unloading. The quantity δ_o is the permanent deformation and is determined as a two parameter curve fit from experimental data. The form used is

$$\delta_o = C\delta_{max}^i \tag{B.3}$$

This quantity represents how deeply the impactor has indented the plate. The quantities K, n, m, C and i must be found experimentally. Yang and Sun, (refs. 16 and 17), have shown that this formulation gives reasonable results for composite plates being impacted by a spherical impactor. If δ becomes less than δ_o, the plate and imoactor have separated, and the contact force is set to zero.

A typical force-deflection diagram is shown in figure B.1. This curve shows a spring that is loading from point A to B. At point B, the plate has undergone a permanent indentation $\delta_{o(1)}$, so that it will unload along curve 2 to point C. At point C, the plate and impactor have separated, allowing further separation to follow curve 3 to point D. Curve 4 shows the gap between the plate

and impactor closing until contact is again made at point C. The spring then loads along curve 5 until it reaches point B. At B, it continues loading along the original curve until point E, where the spring begins to unload again. The plate now has a new permanent indentation $\delta_{o(2)}$, causing the spring to unload along curve 7 to point F, where it reverses and begins to load again. During the course of an impact event, this loading, unloading and separation may occur many times.

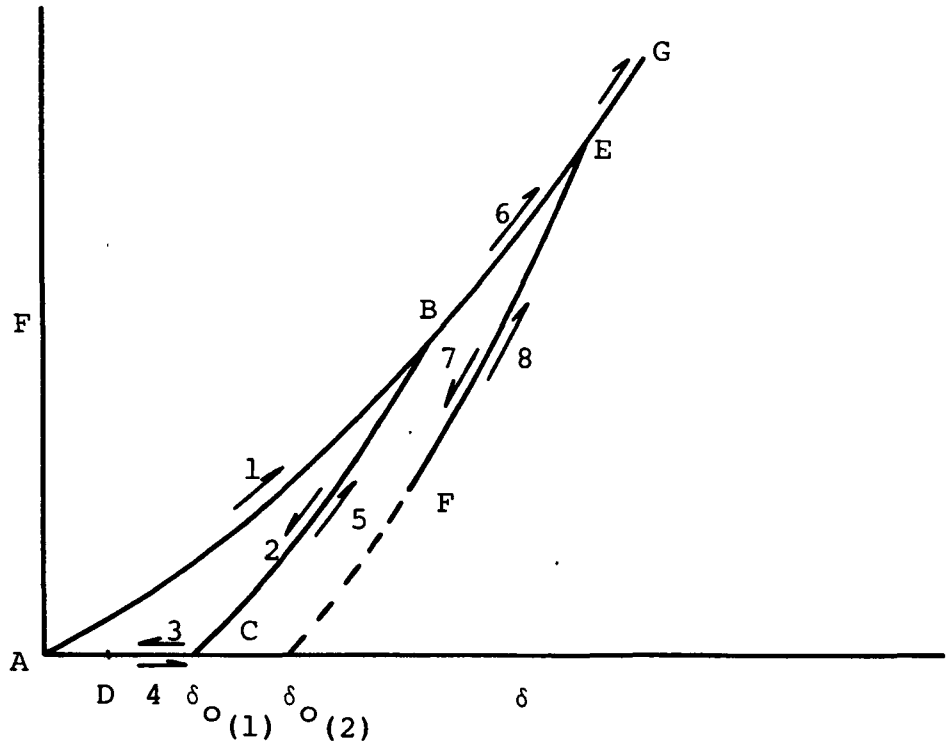

Figure B.1. Typical Force-Deflection Diagram for Nonlinear Contact Spring

APPENDIX C

NUMERICAL SOLUTION OF THE TRANSIENT DYNAMIC PROBLEM

The general form of the equations of motion for a discretized elastic system may be written as

$$[M]\{\ddot{x}\} + [C]\{\dot{x}\} + [K]\{x\} = \{F\} \tag{C.1}$$

where

$[M]$ = mass matrix
$[C]$ = damping matrix
$[K]$ = stiffness matrix
$\{\ddot{x}\}$ = acceleration vector $(\frac{d^2x}{dt^2})$
$\{\dot{x}\}$ = velocity vector $(\frac{dx}{dt})$
$\{x\}$ = displacement vector
$\{F\}$ = applied load vector

This equation represents a set of n simultaneous second order differential equations. This set of n second order equations is most easily solved numerically, if it is rewritten as a set of 2n first order equations. This may be done by defining

$$\{\dot{x}\} = \{y\} \tag{C.2}$$

Substituting (C.2) into (C.1) and solving for $\{\dot{y}\}$ yields

$$\{\dot{y}\} = [M]^{-1}(\{F\}-[C]\{y\} - [K]\{x\}) \tag{C.3}$$

Two assumptions have been made to ease the computational effort. First, the mass matrix is assumed to be diagonal (lumped mass), and secondly, Rayleigh damping is used where the damping matrix is assumed to be related to the mass and stiffness matrices by

$$[C] = \alpha[M] + \beta[K] \tag{C.4}$$

Where the constants α and β are related to the material and structural damping of the system. Incorporating these assumptions into equation (C.3) and combining the result with equation (C.2) gives

$$\begin{Bmatrix} \dot{x} \\ \dot{y} \end{Bmatrix} = \begin{Bmatrix} \{\phi\} \\ [M]^{-1}\{F\} \end{Bmatrix} - \begin{bmatrix} [\phi] & [I] \\ [M]^{-1}[K] & (\alpha+\beta[M]^{-1}[K]) \end{bmatrix} \begin{Bmatrix} x \\ y \end{Bmatrix} \tag{C.5}$$

Since the global stiffness matrix is merely the sum of the individual element stiffness matrices, equation (C.5) may be evaluated by summing the contribution due to each element without ever assembling the global stiffness matrix. The global mass matrix must, however, be assembled. Inversion of the mass matrix is simplified due to the fact that it is diagonal. Internally, CLIP II treats the mass matrix as a vector, which reduces both the storage requirements, and the number of multiplications needed for a matrix multiplication. A computational simple expression for $\dot{y}_i$ may then be written as

$$\dot{y}_i = \frac{1}{M_{ii}} \left(f_i - \sum_{j=1}^{n} K_{ij}x_j - \alpha M_{ii}y_i - \beta \sum_{j=1}^{n} k_{ij}y_j\right) \tag{C.6}$$

Equation (C.5) is now in a form which allows a suitable numerical integration scheme to be used to step out the dynamic solution in time. The scheme used in CLIP II is the fourth order Runge-Kutta-Gill method, and is implemented in the subroutine RKGINT. This integration formula predicts the solution at time i+1 wing

$$\{u\}_{i+1} = \{u\}_i + \frac{\Delta t}{6}[\{K_1\} + 2(1-\frac{1}{\sqrt{2}})\{K_2\} + 2(1+\frac{1}{\sqrt{2}})\{K_3\} + \{K_4\}] \tag{C.7}$$

where

$$\{u\}^T = \{x\ y\}$$

$$\{K_1\} = \{g(t_i, \{u\}_i)\}$$

$$\{K_2\} = \{g(t_i+\tfrac{1}{2}\Delta t,\ \{u\}_i+\tfrac{1}{2}\Delta t\{K_1\})\}$$

$$\{K_3\} = \{g(t_i+\tfrac{1}{2}\Delta t,\ \{u\}_i+(-\tfrac{1}{2}+\tfrac{1}{\sqrt{2}})\Delta t\{K_1\}+(1-\tfrac{1}{\sqrt{2}})\Delta t\{K_2\})\}$$

$$\{K_4\} = \{g(t_i+\Delta t,\ \{u\}_i-\tfrac{1}{\sqrt{2}}\Delta t\{K_2\}+(1+\tfrac{1}{\sqrt{2}})\Delta t\{K_3\})\}$$

and $\{g(t_i, \{u\}_i)\}$ represents equation (C.5) evaluated at time t_i with the solution vector $\{u\}_i$. This evaluation is performed within CLIP II by the subroutine DERIVS. This scheme requires that the initial state of the system, both velocities and displacements, be specified.

The time increment, Δt, may vary from step to step, as only the last solution is required to predict the next solution. If, however, the time increment is relatively large, it may be necessary to periodically correct the predicted solution. This is done in CLIP II by the subroutine CORECT, which incorporates Hamming's fourth order correcting algorithm. This algorithm is of the form

$$\{u\}_{i+1} = \tfrac{9}{8}\{u\}_i-\tfrac{1}{8}\{u\}_{i-2}+\tfrac{3}{8}\Delta t(\{\dot{u}\}_{i+1}+2\{\dot{u}\}_i-\{\dot{u}\}_{i-1}) \qquad (C.8)$$

Notice that equation (C.8) is an implicit formula which requires an iterative solution. Further, it is dependent upon the last three solutions, which requires the time increment to be constant for at least three time steps before the correcting is performed. This procedure is very time consuming, and should only be done if absolutely necessary. Reference 20 provides a good discussion on both the R-K-G predictor and Hamming's corrector.

APPENDIX D
LAMINATE FAILURE CRITERIA

The failure criteria utilized in CLIP II to predict damage are based upon Hashin's failure criteria for unidirectional fiber composites (ref. 23). The criteria allows for the prediction of both the presence of failure and identification of the mode of failure. Modes of failure which can be predicted include fiber breakage, ply splitting parallel to the fibers, and delaminations between plies.

The stresses predicted within CLIP II are depicted in figure D.1. The 1-direction coressponds to the fiber direction in a ply and σ_{13} and σ_{23} stresses are transverse shear stresses. The failure criteria make use of eight material strength parameters which are:

S_{1T} = fiber direction tensile strength

S_{1C} = fiber direction compressive strength

S_{2T} = tensile strength perpendicular to the fibers

S_{2C} = compressive strength perpendicular to the fibers

S_{12} = shear strength in the 1-2 plane

S_{13} = shear strength in the 1-3 plane

S_{23} = shear strength in the 2-3 plane

S_{IF} = interlaminar shear strength

The failure criteria are separated into the three different modes. For fiber breakage, the criteria are

$$\left(\frac{\sigma_{11}}{S_{IT}}\right)^2 + \left(\frac{\sigma_{12}}{S_{12}}\right)^2 + \left(\frac{\sigma_{13}}{S_{13}}\right)^2 = 1 \qquad \text{(D.1)}$$

at failure for $\sigma_{11} > 0$, and

$$\left(\frac{\sigma_{11}}{S_{1C}}\right)^2 = 1 \qquad \text{(D.2)}$$

at failure for $\sigma_{11}<0$.

For predicting splitting parallel to the fibers, the criteria are

$$\left(\frac{\sigma_{22}}{S_{2T}}\right)^2 + \left(\frac{\sigma_{23}}{S_{23}}\right)^2 + \left(\frac{\sigma_{12}}{S_{12}}\right)^2 + \left(\frac{\sigma_{13}}{S_{13}}\right)^2 = 1 \qquad \text{(D.3)}$$

at failure for $\sigma_{22} > 0$, and

$$\frac{1}{S_{2C}}\left[\left(\frac{S_{2C}}{2S_{23}}\right)^2 - 1\right]\sigma_{22} + \left(\frac{\sigma_{22}}{2S_{23}}\right)^2 + \left(\frac{\sigma_{23}}{S_{23}}\right)^2 + \left(\frac{\sigma_{12}}{S_{12}}\right)^2 + \left(\frac{\sigma_{13}}{S_{13}}\right)^2 = 1 \qquad \text{(D.4)}$$

at failure for $\sigma_{22} < 0$.

Delaminations are predicted utilizing a simple quadratic interaction formula:

$$\frac{\sigma_{13}^2 + \sigma_{23}^2}{S_{IF}^2} = 1 \qquad \text{(D.5)}$$

at failure.

In the prediction of failure, equations (D.1) - (D.4) are evaluated at the top, middle and bottom of each ply in the laminate and equation (D.5) is evaluated at both the top and bottom of each ply.

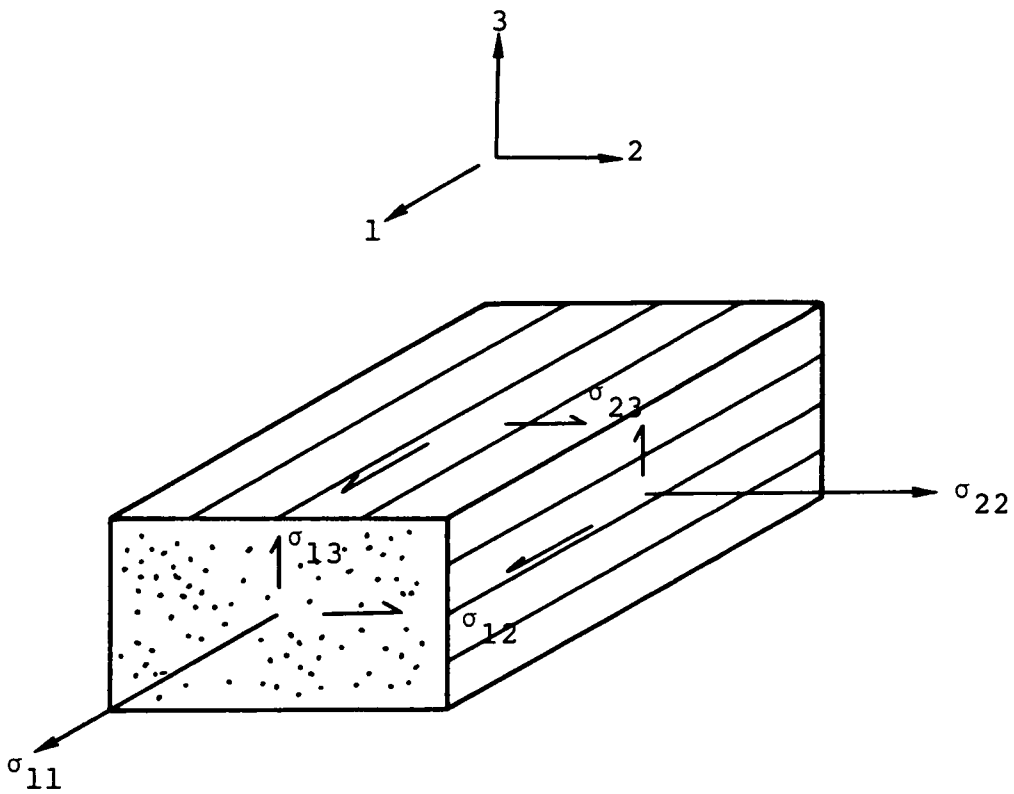

Figure D.1. Stress Components

APPENDIX E

INCORPORATION OF DELAMINATION EFFECTS

The methodology adopted for incorporating the effects of damage in the impact analysis involves modification of the elemental stiffness matrices. For the case of ply damage, the reduction in stiffness is accounted for simply by specifying appropriate ply moduli as zero and reformulating the laminate constitutive matrices.

Elemental modifications to account for delaminations are not so easily defined since the result of a delamination is a change in both the bending and transverse shear stress distributions. The change in bending stress is a function of the presence of shear and hence the two are coupled. A delamination does not affect the stiffness of a bending element in the presence of pure bending.

Consider a homogeneous beam with a central delamination subjected to pure bending (no shear). Since there are no shear stresses, the plane of the delamination is stress free. Thus, the delamination can have no effect on the stress field or bending rigidity.

If a homogeneous beam is subjected to combined bending and shear, the resulting stresses are those depicted in figure E.2. The parabolic shear stress distribution is characteristic of the linear bending stress distribution. When a delamination is introduced, the bending and shear stresses must change, primarily because the shear stresses must vanish at the delamination.

The bending stresses in the delaminated beam subjected to both bending and shear are shown in figure E.3. In addition to the expected bending stress variation, singular forces at the ends of the delamination are present which balance the difference in total force at each end of the delaminated beam. Thus, horizontal equilibrium is maintained. Since the magnitude of the singular forces balances the force imbalance in bending, the singular force is simply the shear force which existed on the plane of the delamination prior to the delamination.

The stresses depicted in figure E.3 can be separated into two parts consisting of a normal bending stress distribution and a membrane stress distribution. This has been done in figure E.4. The magnitude of the singular forces is now seen to be simply the difference in membrane force along the length of the partial beams.

The moments depicted in figure E.4 must be balanced by the transverse shear forces. Without consideration of the singular forces, the moment gradients depicted are not in balance with the shear forces. This is remedied by distributing the singular forces over the partial beams as depicted in figure E.5. The singular forces have been moved to the midsurfaces of the two partial beams and moments added to account for the change in the line of action of the moved forces. The result of the moments added serves to increase the moment gradients across the length of the partial beams. This occurs since the smaller end moments have been reduced while the larger end moments have been increased. It can be shown that the moment gradients are now equal to the shear force and hence the model is in equilibrium. The resulting bending stress distributions are depicted in figure E.6. Shear stresses are also shown in figure E.6. The peak shear stresses are identical to those shown in figure E.2.

The model described for the effect of bending and shear in the presence of a delamination has been utilized to define properties of a composite laminate with a delamination. The development of the analysis for a laminate requires the partial laminate constitutive relations and expressions for transverse shear stresses as a function of the average rotation.

Utilizing the work of Cohen (ref. 19), the relation between interlaminar shear stress and transverse shear rotation is defined as

$$\begin{Bmatrix} \tau_{xz} \\ \tau_{zy} \end{Bmatrix}^{i} = [R]^{i} = \begin{Bmatrix} \gamma_{xz} \\ \gamma_{yz} \end{Bmatrix} \tag{E.1}$$

where $\{^{\gamma_{xz}}_{\gamma_{yz}}\}$ are average shear rotations and the superscript "i" identifies the location through the thickness. Using (E.1), singular forces due to a delamination at interface "i" can be determined as

$$F_x^s = \int_A \tau_{xz}\, dA$$

and

$$F_y^s = \int_A \tau_{xz}\, dA$$

or

$$\begin{Bmatrix} F_x^s \\ F_y^s \end{Bmatrix} = [R]^i \int_A \begin{Bmatrix} \gamma_{xz} \\ \gamma_{yz} \end{Bmatrix} dA \qquad \text{(E.2)}$$

In the CLIP II code, stresses are computed as an average over the element so that equations (E.2) reduce to

$$\begin{Bmatrix} F_x \\ F_y \end{Bmatrix}^i = [R]^i \begin{Bmatrix} \gamma_{xz} \\ \gamma_{yz} \end{Bmatrix} A^e \qquad \text{(E.3)}$$

where A^e is the planar area of the element.

The forces defined in (E.3) are converted into stress and moment resultants in a fashion similar to that shown in figure E.4. Stress resultants become

$$\begin{Bmatrix} N_x^s \\ N_y^s \end{Bmatrix} = \begin{Bmatrix} 1/\Delta y & F_s \\ 1/\Delta x & F_y \end{Bmatrix} \qquad \text{(E.4)}$$

where Δx and Δy are the elemental widths in the x and y directions. The requirement that elements to be monitored for stress be defined as shown in figure 1 stems from the use of equations (E.4) and the need to define Δx and Δy for an element.

Moment resultants are defined as

$$\begin{Bmatrix} M_x^s \\ M_y^s \end{Bmatrix} = (Z_s - Z_i) \begin{Bmatrix} N_x \\ N_y \end{Bmatrix} \tag{E.5}$$

where Z_i is the location of the delamination and Z_s is the mid-surface of the partial laminate either above or below the delamination (fig. E.7).

The stress resultants (E.4) and moment resultants (E.5) are applied, half at each end, to the partial laminates with a linear variation, plus to minus, similarly to that shown in figure E.4. Applying half at each end implies that the singular forces are distributed equally at each end of the delamination.

Using the stress and moment resultants, strains and curvatures are defined using constitutive relations for the partial laminates. Thus

$$\begin{Bmatrix} \varepsilon_x^s \\ \kappa_x^s \end{Bmatrix} = \begin{bmatrix} A & B \\ B & D \end{bmatrix} -1 \quad \begin{Bmatrix} N_x^s \\ M_x^s \end{Bmatrix} \tag{E.6}$$

These strains and curvatures are then utilized in defining the variation of strain through the thickness of the total laminate. The strain distribution through a plate with a delamination takes the form

$$\varepsilon = \varepsilon_o + Z\kappa + \varepsilon^s + (Z - Z_s)\kappa^s \tag{E.7}$$

where ε^s and κ^s may be different for the various sublaminates. Thus, the strains are piecewise linear through the thickness of a delaminated plate element.

This poses a fundamental problem in the plate element since different curvatures are allowed at different locations through the thickness and because jump discontinuities are allowed in strain through the thickness. Neither of these phenomena can be handled with a single plate element modelling all of the sublaminates. To model these effects properly requires a separate plate element for each sublaminate. This approach leads to modelling each ply in the laminate as a separate plate element which then becomes such a large finite element model as to be deemed impossible to utilize.

The approach taken has been to include the strains and curvatures due to the singular forces while maintaining a single value for total rotation and midplane deformation. This leads to an effective reduction in the total rigidity of an element thus incorporating the effects of a delamination.

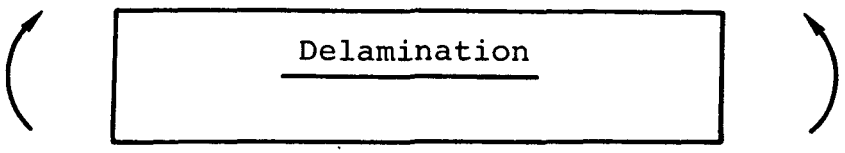

Figure E.1. Beam with Delamination

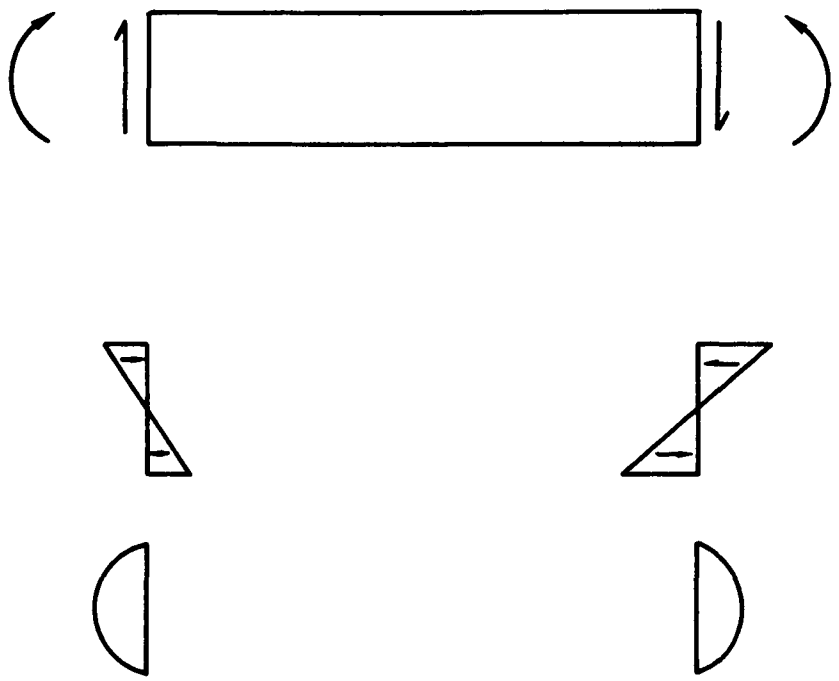

Figure E.2. Bending and Shear Stresses

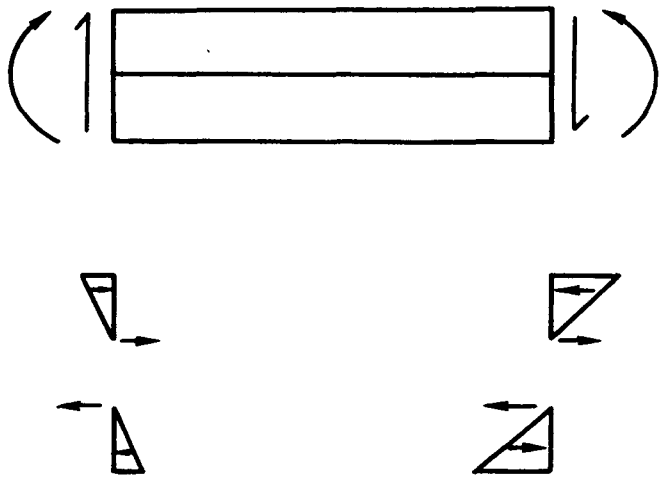

Figure E.3. Bending and Shear with a Delamination

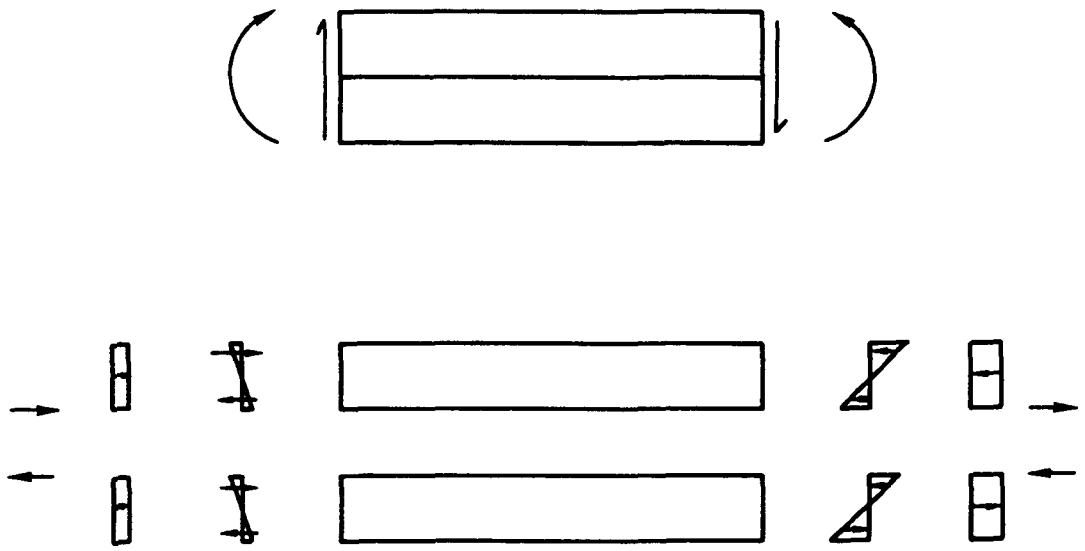

Figure E.4. Decomposition of Bending Stresses with Shear and a Delamination

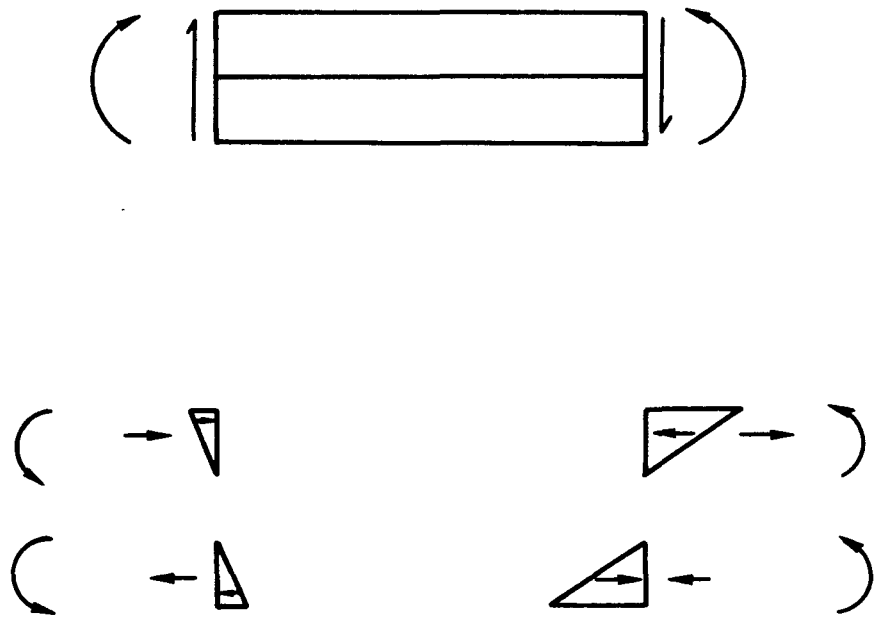

Figure E.5. Distributing Singular Shear Forces

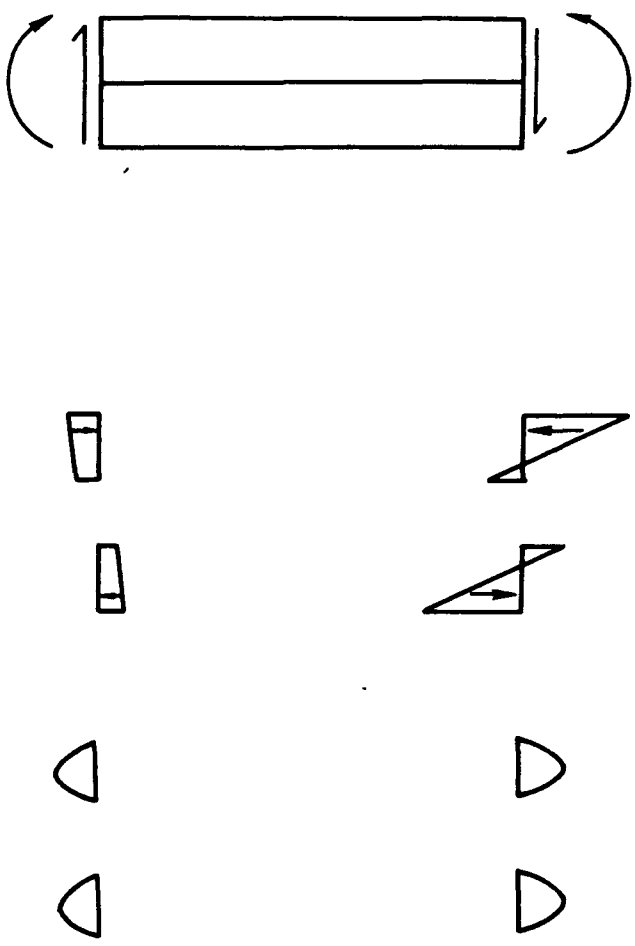

Figure E.6. Bending and Shear Stresses with a Delamination

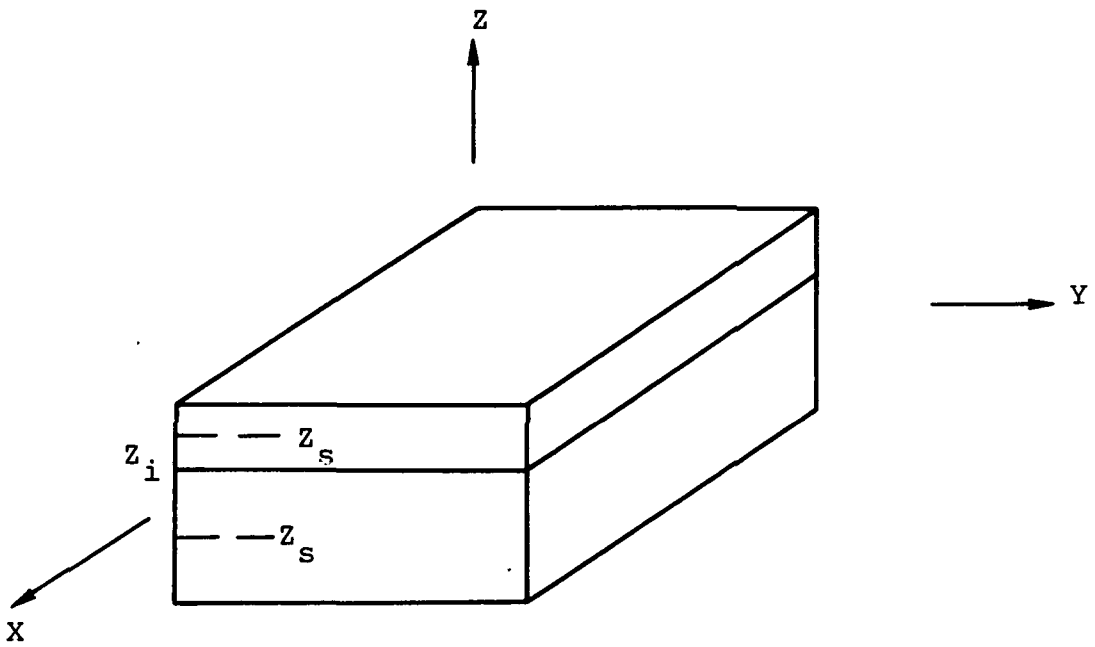

Figure E.7. Delaminated Plate

APPENDIX F

CLIP II PROGRAM USER'S GUIDE

I. PROGRAM CONTROL DATA

Card 1		Title Card	20A4
Columns		Contents	
1-80	TITLE(20)	80 character alphanumeric title	

Card 2		Save & Restart Flags	215A
Columns		Contents	
1-5	IREST	If IREST=0, this is a new analysis	
		If IREST=1, restart the analysis from FILEØ8	
6-10	ISAVE	If ISAVE=0, do not generate restart file (FILEØ8)	
		If ISAVE=1, generate a restart file	

Card 3		Step Control Data	3I5
Columns		Contents	
1-5	NTSTEP	The number of time steps to be taken	
6-10	NPRINT	The number of time steps per solution printout (every NPRINTth time step will be printed)	
11-15	NSTRES	The number of time steps per stress analysis (a stress analysis will be performed after NSTRES time steps)	

Card 4		Printout Control Flags	4I5
Columns		Contents	
1-5	LAMPRT	Lamina stress-strain matrix printout flag	
6-10	VELPRT	Velocity printout flag	
11-15	ACCPRT	Acceleration printout flag	
16-20	STRPRT	Detailed stress printout flag	
		For any of the above flags, a value of 1 turns on the printout option, and a value of Ø suppresses the the printout	

I. PROGRAM CONTROL DATA (continued)

Card 5		Time Step Data	2F10.0
Columns		Contents	
1-10	TIME	The initial time	
11-20	DELT	The time increment	

Card 6		Correcting Algorithm Control Data	2I5, F10.0
Columns		Contents	
1-5	NCOREC	The number of time steps per correcting step. If NCOREC=Ø, no correcting will be performed	
6-10	NITMAX	The maximum number of iterations per correcting step	
11-20	CONV	The corrector convergence criterion	

Card 7		Stiffness Integration Control	I5
Columns		Contents	
1-5	IORDER	The order of the numerical integration used to evaluate the element stiffness matrices, may be either 2 or 3	

II. MATERIAL DESCRIPTION INPUT

Card 1		Number of Materials	I5
Columns		Contents	
1-5	NMAT	The number of different materials used in the laminate. $0<NMAT\leq 5$	

II. MATERIAL DESCRIPTION INPUT (continued)

Card 2	Material Properties for Material 1	7F10.0
Columns		Contents
1-10	E1	Longitudinal Young's modulus
11-20	E2	Transverse Young's modulus
21-30	NU12	Poisson's ratio in the 1-2 plane (load-strain)
31-40	G12	Shear modulus in the 1-2 plane
41-50	G13	Shear modulus in the 1-3 plane
51-60	G23	Shear modulus in the 2-3 plane
61-70	RHO	Density

Card 3	Strengths of Material 1	8F10.0
Columns		Contents
1-10	S1C	Longitudinal compressive strength
11-20	S1T	Longitudinal tensile strength
21-30	S2C	Transverse compressive strength
31-40	S2T	Transverse tensile strength
41-50	S12	Shear strength in the 1-2 plane
51-60	S13	Shear strength in the 1-3 plane
61-70	S23	Shear strength in the 2-3 plane
71-80	SIF	Interfacial shear strength

If more than one material is used, cards 2 and 3 are repeated NMAT times.

III. LAMINATE DESCRIPTION INPUT

Card 1	Number of Plies	I5
Columns		Contents
1-5	NPLY	The number of plies in the laminate. $0<NPLY\leq 25$

III. LAMINATE DESCRIPTION INPUT (continued)

Card 2	Ply Description	2F10.0, I5
Columns		Contents
1-10	THICK(I)	The thickness of ply 1
11-20	THETA(I)	The orientation of ply 1, measured counterclockwise from the positive x axis
21-25	MID	The I.D. number of the material used for ply 1

Card 2 is repeated NPLY times.

IV. DAMPING INPUT

Card 1	Damping Parameters	2F10.0
Columns		Contents
1-10	ALPHA	The mass matrix multiplier
11-20	BETA	The stiffness matrix multiplier

V. NODAL COORDINATE INPUT

Card 1	Number of Nodes	I5
Columns		Contents
1-5	NN	The number of nodes used in the model

Card 2	Coordinate Input	I5, 2F10.0
Columns		Contents
1-5	N	Node number. N is only used for clarity when looking at the coordinate input. The M^{th} coordinate card will be used for the coordinates of node M regardless of the value of N.
6-15	X	The X coordinate of node N
16-25	Y	The Y coordinate of node N

Card 2 will be repeated NN times.

VI. CONSTRAINED DEGREE OF FREEDOM INPUT

Card 1		Number of Constrained Nodes	I5
Columns		Contents	
1-5	NCDF	The number of nodes constrained in direction 1 (global x direction)	

Card 2		Constrained Nodes	15I5
Columns		Contents	
1-5	ICDF(1)	1st node constrained in direction 1	
6-10	ICDF(2)	2nd node constrained in direction 2	
.	.	.	
.	.	.	
.	.	.	
71-75	ICDF(15)	15th node constrained in direction 3	

Card 2 is repeated until NCDF nodes have been specified.

Card sets 1 and 2 are repeated for directions 2, 3, 4 and 5.

Direction	Degree of Freedom
1	X
2	Y
3	Z
4	θ_x
5	θ_y

VII. ELEMENT DEFINITION INPUT

Card 1		Number of Elements	I5
Columns		Contents	
1-5	NE	The number of elements used in the model	

VII. ELEMENT DEFINITION INPUT (continued)

Card 2		Element Definition	9I5
Columns		Contents	
1-5	NI	1st node in the element definition	
6-10	NJ	2nd node in the element definition	
.	.	.	
.	.	.	
.	.	.	
36-40	NP	8th node in the element definition	
41-45	MON	Stress analysis monitor. If MON=0, no stress analysis will be performed for this element; if MON=1, stresses will be calculated.	

Card 2 is repeated NE times.

VIII. INITIAL CONDITION INPUT

Card 1		Number of Specified Displacements	I5
Columns		Contents	
1-5	NID	The number of nodes at which non-zero initial displacements will be specified	

Card 2		Displacement Specification	I5, 5F10.0
Columns		Contents	
1-5	N	Node at which displacements are specified	
6-15	X(N,1)	Displacement in direction 1 for node N	
16-25	X(N,2)	Displacement in direction 2 for node N	
26-35	X(N,3)	Displacement in direction 3 for node N	
36-45	X(N,4)	Displacement in direction 4 for node N	
46-55	X(N,5)	Displacement in direction 5 for node N	

Card 2 is repeated NID times.

Cards 1 and 2 are repeated for initial velocity input.

IX. IMPACT PARAMETERS

Card 1		Impactor & Contact Spring Input	I5, 8F10.0
Columns		Contents	
1-5	N	The node at which the contact spring is connected	
6-15	MASS	The mass of the impactor	
16-25	K	The spring rate for loading	
26-35	N	The spring exponent for loading	
36-45	M	The spring exponent for unloading	
46-55	I	The permanent deformation exponent	
56-65	C	The permanent deformation multiplier	
66-75	Xo	The initial position of the impactor	
76-85	Vo	The initial velocity of the impactor	

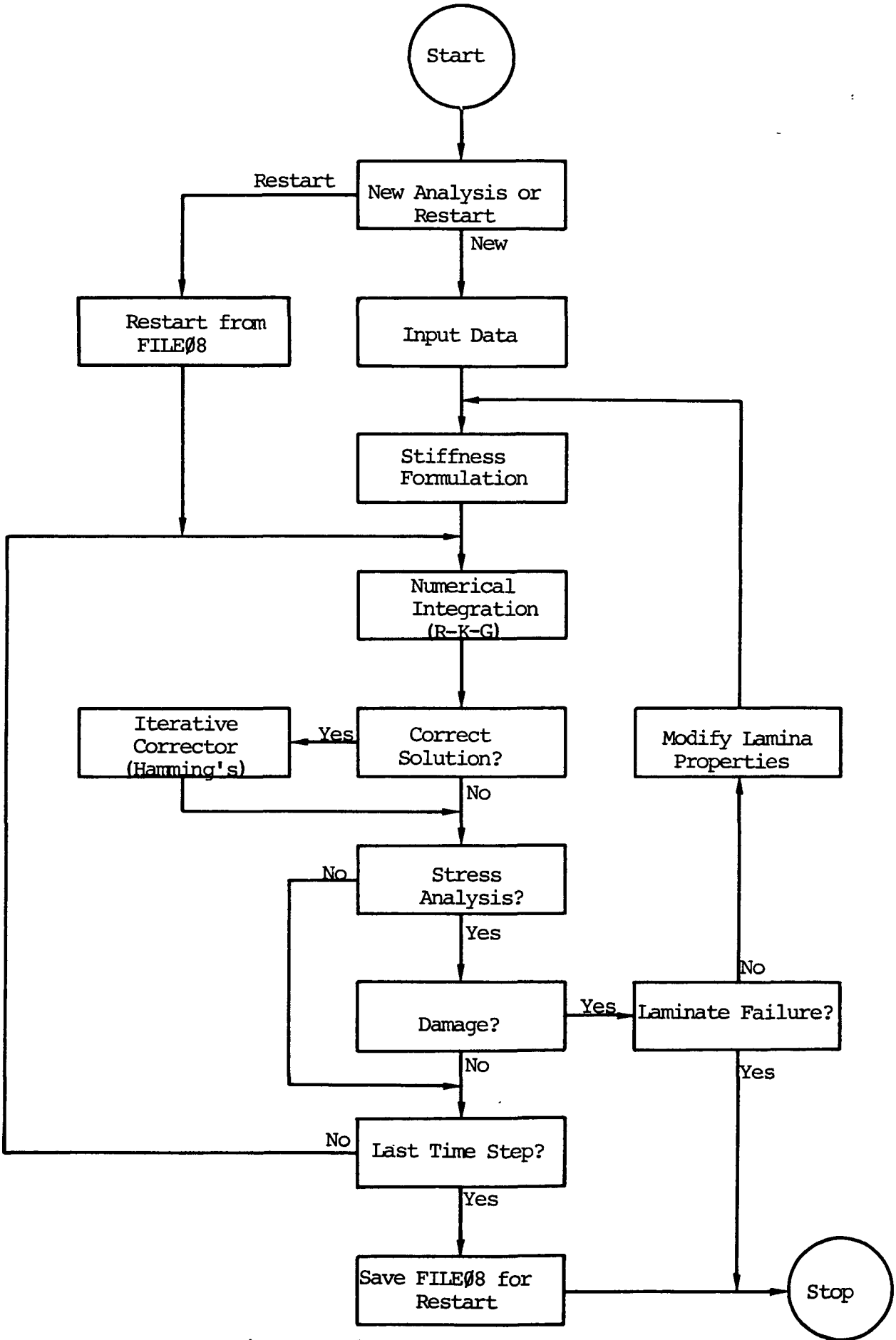

Figure F.1. CLIP II Flow Chart

NASA Contractor Report 166086
Distribution List
NAS1-15888

	No. Copies
NASA Langley Research Center Hampton, VA 23665	
Attn: Research Information Office, Mail Stop 151A	1
Technology Utilization Office, Mail Stop 139A	1
Dr. James H. Starnes, Mail Stop 190	1
Walter Illg, Mail Stop 188E	10
NASA Ames Research Center Moffett Field, CA 94035	
Attn: Library, Mail Stop 202-3	1
NASA Ames Research Center Dryden Flight Research Facility P. O. Box 273 Edwards, CA 93523	
Attn: Library	1
NASA Goddard Space Flight Center Greenbelt, MD 20771	
Attn: Library	1
NASA Lyndon B. Johnson Space Center 2101 Webster Seabrook Road Houston, TX 77058	
Attn: JM6/Library	1
NASA Marshall Space Flight Center Marshall Space Flight Center, AL 35812	
Attn: Library, AS24L	1
Jet Propulsion Laboratory 4800 Oak Grove Drive Pasadena, CA 91103	
Attn: 111-113/Library	1
NASA Lewis Research Center 21000 Brookpark Road Cleveland, OH 44135	
Attn: Library, Mail Stop 60-3	1
NASA John F. Kennedy Space Center Kennedy Space Center, FL 32899	
Attn: Library, NWSI-D	1
National Aeronautics and Space Administration Washington, DC 20546	
Attn: RTH-6	1

	No. Copies
Illinois Institute of Technology Mechanical Engineering Department Attn: Dr. I. M. Daniel Chicago, IL 60616	1
Purdue University School of Aeronautics and Astronautics Attn: Professor C. T. Sun West Lafayette, IN 47907	1
IIT Research Institute Attn: Mr. Scott W. Schramm 10 West 35th Street Chicago, IL 60616	1
NASA Scientific and Technical Information Facility 6571 Elkridge Landing Road Linthicum Heights, MD 21090	25 plus original

1. Report No.	2. Government Accession No.	3. Recipient's Catalog No.
NASA CR-166086		

4. Title and Subtitle	5. Report Date
DEVELOPMENT OF AN ANALYTIC PROCEDURE TO CALCULATE DAMAGE ACCUMULATION IN COMPOSITES DURING LOW VELOCITY IMPACT	May 1983
	6. Performing Organization Code

7. Author(s)	8. Performing Organization Report No.
E. A. Humphreys and J. Goering	MSC TFR 1315/0208
	10. Work Unit No.

9. Performing Organization Name and Address	11. Contract or Grant No.
Materials Sciences Corporation Gwynedd Plaza II, Bethlehem Pike Spring House, PA 19477	NAS1-15888
	13. Type of Report and Period Covered Contractor Report 8/3/79 - 4/15/83

12. Sponsoring Agency Name and Address	14. Sponsoring Agency Code
National Aeronautics & Space Administration Langley Research Center Hampton, VA 23665	

15. Supplementary Notes

Final Report

16. Abstract

A computerized procedure was developed to model the response of a laminated composite plate subjected to low velocity impact. The methodology incorporated transient dynamics finite element analysis coupled with composite layer and interlaminar stress predictions. Damage was predicted using a stress based failure criteria and incorporated into the solution as stiffness modifictions. The force-displacement relation between the impactor and plate was modelled with a nonlinear contact spring similar to Hertzian contact. Analyses performed predicted ply damage early in the impact event when the displacement fields were characteristic of high frequency flexural response.

17. Key Words (Suggested by Author(s))	18. Distribution Statement
Composites, Impact, Damage Modelling, Graphite/Epoxy	Unclassified - Unlimited

19. Security Classif. (of this report)	20. Security Classif. (of this page)	21. No. of Pages	22. Price
Unclassified	Unclassified	85	